NASA-CR-194407

California Polytechnic State University
San Luis Obispo, CA 93407

IN-02-CR
OCIT
186234
52 P

Numerical Prediction of Transition of the F-16 Wing at Supersonic Speeds

Final Report
September 1993

Russell M. Cummings and Joseph A. Garcia
Aeronautical Engineering Department

CHAPTER 1

INTRODUCTION

1.1 Background

1.1.2 Laminar Flow Control

Extending Laminar flow in reality is the delay of boundary layer transition. This control is obtained by passive, active, or reactive techniques [1]. Passive techniques, also know as Natural Laminar Flow control (NLF), are categorized as those means of altering the flow through normal aerodynamic control parameters, for example:

- pressure-gradient
- wall shaping
- sweep
- angle of attack
- Reynolds number

Active techniques are categorized as those means of altering the flow through outside applied means, for example:

- wall suction
- heat transfer

A third form of flow control is reactive flow control. Reactive flow control is the process by which out-of-phase disturbances are artificially introduced into the boundary layer to cancel those disturbances already present, thus stabilizing the flow and delaying transition. Some reactive controls include periodic heating/cooling, and wall motion. However, this method of Laminar flow control is complex and to date is more of a theoretical method.

The underlying principle of these techniques, as one expert puts it, is:

"The realization that transition is the eventual stage
in a process that involves amplification of disturbances
in the boundary layer" [1].

Prediction of boundary-layer transition is an area which requires reliable methods and must be sensitive to any control parameter that alters the mean flow. These parameters include the active, passive, and reactive flow controls mentioned above.

1.1.3 Transition

The Transition process is composed of several physical processes as described in figure 1.1 [1]. External disturbances are internalize through a viscous process know as "receptivity" [2]. Some of these external disturbances include freestream vorticity, surface roughness, vibrations and sound. Identifying and defining the initial disturbance for a given problem is the bases for the prediction of transition and creates an initial value problem. The initial disturbance is a function of the type of flow in consideration as well as its environment and therefore is not usually known [1].

The disturbances in the boundary layer eventually enter the critical layer which then amplify and can be modeled by linear stability theory. The modes responsible for the amplification of these disturbances in boundary layer flow are Tollmein Schlichting (viscous) waves or T-S waves, Rayleigh (inflectional) waves (i.e. instabilities due crossflow or high Mach numbers), and Gortler vortices for curved streamlines [1].

Once the amplifications are large enough, nonlinearity sets in through secondary and tertiary instabilities and the flow becomes "transitional" [1]. It should be noted that the nonlinear portion of the flow is small compared to the linear region and therefore can still often be approximated by linear stability

theory for preliminary designs. One thing that must be avoided in all laminar flow studies is the introduction of high levels of initial nonlinear disturbances, which cause a bypass of the linear disturbance regime and yields an almost instantaneous transition. An example of such a nonlinear transition is attachment-line contamination, and is commonly found in swept wings due to the high crossflow at the wing leading edge.

1.2 Previous Work

Laminar flow control began in the 1930's with studies which investigated methods of Natural Laminar Flow control (NLF), specifically pressure gradient flows. This research led to the development of the NACA6-series airfoils in the 1940's. Natural Laminar flow research was later halted in the 1950 by the development of high speed jet engine aircraft. These jet aircraft reached transonic/supersonic speeds requiring the wing to be swept to obtain lower local mach numbers and maintain reasonable aircraft performance [3]. The effect of sweeping the wing then introduces a three dimensional, crossflow, instability that eliminates the ability to maintain laminar flow through current means. The sweep back and highly favorable pressure gradient near the leading-edge of the wing induces a boundary layer crossflow. The sweep and adverse pressure gradient near the trailing edge likewise induces crossflow instabilities on the trailing edge portion of the wing. Unlike the more common "viscous" two dimensional Tollmein Schlighting (TS) instabilities, which are damped when a favorable pressure gradient is applied, the three dimensional crossflow "inflectional" instabilities are amplified when such a favorable pressure gradient is applied [4].

Natural laminar flow control research would now be replaced by attempts to actively control boundary-layer transition, more commonly known as Laminar Flow Control (LFC). These types of controls are categorized as active flow

control which began with flow suction on swept wings. Work in this area peaked in the 1960's with the flight test of the X-21A. The X-21A's work showed the basic feasibility of extending LFC through active flow techniques at Reynolds number as high as 30×10^6 [5].

Further development of the current research in LFC were delayed for a period of about 10 years due to the lack of necessity for improving aircraft fuel efficiency due to both the abundance of low cost fuel resource and the high cost of designing such capabilities. It was not until the 1970's that interest in LFC research was recaptured and has continued to the present day.

The need for higher fuel efficient aircraft has further forced aircraft designers to look at fuel efficiency as there top requirement. A major factor affecting fuel efficiency is aerodynamic drag. More specifically, turbulent skin friction drag. Advancements in super computers and computing methods have led to the analysis of the boundary-layer transition stability problem and the ability to develop manufacturing processes to create the needed aircraft skin material to include strength as well as smoothness. Therefore, laminar flow has become a more realistic method of improving aircraft fuel efficiency.

Reducing the turbulent skin friction is done by extending the amount of laminar flow over the aircraft. Until recently, most studies on laminar flow have been in the subsonic flow region. Work done in this subsonic realm has shown that turbulent skin friction drag can contribute as much as 50% of the total aircraft drag [6]. Studies on typical Supersonic Transports (SST) have shown the potential increase in cruise Lift-to-drag ratio with increase laminar flow [7-8]. Other benefits of laminar flow at supersonic speeds include aerodynamic heating reduction, which allows for an increase option of skin/structure material therefore, decreasing the aircraft gross weight and increasing it's range/payload capability.

1.2 Current Work

A parametric study is being conducted as an effort to numerically predict the extent of natural laminar flow (NLF) on finite swept wings at supersonic speeds. This study is one aspect of a High Speed Research Program (HSRP) to gain an understanding of the technical requirements for high-speed aircraft flight.

As mentioned previously, by extending laminar flow over the skin of an aircraft, there is a significant decrease in the turbulent skin friction, which in turn decreases the total drag force on the aircraft's body. Furthermore, extending laminar flow at supersonic speeds will also significantly decrease the surface temperatures allowing for a more optimum selection of skin material.

Therefore, by understanding the nature of laminar flow and the ability to control laminar flow, the following benefits can be expected in future aircraft designs:

1) Increase range
2) Increase payload
3) Decrease fuel requirement
4) Increase options for skin material
5) Decrease initial cost
6) Decrease operating cost

The parameters that are being addressed in this study are Reynolds number, angle of attack, and leading-edge wing sweep. These parameters were analyzed through the use of an advanced Computation Fluid Dynamics (CFD) flow solver, specifically the Ames Research Center's Three Dimensional Compressible Navier Stokes (CNS) flow solver [9]. From the CNS code, pressure coefficients (Cp) are obtain for the various cases. These Cp's are then used to compute the boundary-layer profiles through the use of the "Kaups and Cebeci" compressible two-dimensional boundary layer code (Wing) [10]. Finally

the boundary-layer parameters are processed into a three dimensional compressible boundary layer stability code (COSAL) to predict transition [11].

The parametric study then consisted of four geometries which addressed the effects of sweep, and three angle of attacks from zero to ten degrees to yield a total of 12 cases. The above process was substantially automated through a procedure that was developed by the work conducted under this study. This automation procedure then yields a three dimensional graphical measure of the extent of laminar flow by predicting the transition location of laminar to turbulent flow.

CHAPTER 2

GOVERNING EQUATIONS

2.1 Mean Flow

The physics of the flow in consideration can be described by the fundamental equations governing viscous fluid flow. These fundamental equations are based upon the universal laws of conservation of mass, momentum, and energy. These conservation laws are used to formulate the time-averaged, non dimensional Navier-Stokes equations, in Cartesian coordinates (X,Y,Z) [9].

2.1.2 THIN - LAYER APPROXIMATION

Large amounts of CPU time are necessary to solve the time-averaged three-dimensional Navier-Stokes equations. Particularly for flow about realistic geometries. To alleviate some of this large (CPU) requirement a thin-layer approximation is applied to the governing equations. The thin-layer approximation is applicable to high Reynolds number flows where the boundary layer is thin and assumes that the effects of viscosity are concentrated near the rigid boundaries and only vary in the wall-normal direction. It should be noted that the thin-layer approximation requires that the body surface be mapped to a coordinate surface and that clustering be normal to this surface. The resulting grid resolution usually has fine grid spacing in the normal body direction and coarser spacing along the body. Therefore, the viscous terms in the normal body direction are preserved and those viscous terms in the stream and spanwise direction are neglected. This approximation yields a simplified version of the Navier Stokes equation [9].

2.2 Boundary Layer Equations

To determine the boundary layer transition stability, the use of a boundary code "Wing" was used. A conical flow approximation for the flow over a finite swept wing is assumed and a polar coordinate system is used as shown in figure 2.1 [10] to simplify the computation. This assumption is valid for pressure isobars along constant percent chord lines or along generators if the wing is of a trapezoidal planform. It should be noted that this assumption is not valid near the tip or root of the wing due to the shock waves created here.

2.3 LINEAR STABILITY EQUATIONS:

A Compressible Stability Analysis code (COSAL) is used to analyze the stability of the three-dimensional boundary layer [11]. The three dimensional viscous incompressible flow can be expressed by the nonlinear Navier Stokes equations. The fluid motion is then decomposed into a steady flow and an instantaneous perturbation where, U is the mean flow velocities in x,y,z.

Next, the perturbations are substituted into the linearized Navier Stokes equations and the assumption of a "quasiparallel" flow is made. It should be noted that a "quasiparallel" flow implies that the mean flow is only a function of the body-normal coordinate "y" for a given point along the body. This assumption is applicable to boundary-layer flows since, at high Reynolds numbers, the flow gradient in the streamwise x-direction are much smaller than in the body normal y-direction. The linear Navier Stokes equation then become separable PDE's where by a normal mode solution is applicable and a disturbance level measurement of the boundary layer flow called the "N-Factor" can be obtain to determine transition. Transition is then predicted empirically at an N-factor of 8 to 10 based on previous studies in swept wings [4,24,25].

CHAPTER 3

NUMERICAL METHODS

The finite difference schemes used in the Compressible Navier Stokes (CNS) code to solve the mean flow governing equations is the implicit approximation factorization algorithm in delta form by Beam and Warming [12].

The basic numerical algorithms used to solved the governing mean flow equations have been taken from the Pulliam-Steger ARC3D computer code [13] and applied to the Compressible Navier Stokes (CNS) code. This algorithm is known as the Pulliam-Chaussee Diagonal ADI Algorithm. This scheme uses the fourth-order-accurate smoothing operator on both the left- and right-hand sides.

CHAPTER 4

COMPUTATIONAL GRID AND BOUNDARY CONDITIONS

4.1 Wing Grid Configurations

The computational grids used in this analysis were generated from an algebraic surface grid generation code developed under this study. The airfoil ordinates, required by the above surface grid code, were obtain from a code called "sixseries" [15]. Sixseries produces the ordinates for airfoils of any thickness, thickness distribution, or camber in the NACA 6- and 6a-series. These ordinates are then redistributed using either the S3D [16] or VG [17] code. Once the desired airfoil section is acquired and the surface grid is generated, the 3D grid is then generated through the use of a hyperbolic volume grid generator called "HYPGEN".

4.1.1 Surface Grid Generator

An algebraic surface grid generation code was developed in order to create various wings geometries. This code generates single-element type wings of various wing sweeps and taper ratios for a given airfoil shape. Appendix A-1 contains a copy of the code along with several pre-processing codes and a list of the procedure to obtain a surface grid. The surface grid generator was designed to allow the user a quick method of creating the mentioned wing surfaces. The following is a list of the inputs:

- Taper Ratio (optional)
- Aspect Ratio (optional)
- Leading Edge or Quarter chord sweep
- Number of spanwise points (cuts) on the wing
- Initial spacing in the spanwise direction
  (tip chord spacing)
- Final spacing in the spanwise direction

(root chord spacing)
- Airfoil ordinate input file obtained from the Wing
Surface Grid Creation procedure shown in appendix A-1.

It should be noted that the process necessary to obtain the above
mentioned airfoil ordinate input file requires a few steps. For a detail explanation
of the process to obtain the airfoil ordinate input file, refer to the procedure listed
in appendix A-1.

The surface grid generation code runs in the order of a few seconds on
the IRIS workstation. One feature of the code includes a check for negative
trailing edge sweep, which can be obtain when certain combination of taper ratio,
aspect ratio, and leading edge sweep are chosen. The reason for this check is
due the fact that the boundary-layer code currently being used in the transition
analysis can not analysis swept forward wing edges.

Finally, it is noted that the algebraic surface grid generator uses the
vinokur stretching routine to cluster points along the spanwise directions at the
wing's wake, root, and tip sections [17a].

4.1.2 Volume Grid Generator
The three dimensional computational grids for the various wing geometries
being studied are generated using a hyperbolic three dimensional grid generation
code HYPGEN [14]. This code generate a 3D volume grid over the above
generated single-block surface grids. HYPGEN accomplishes this my solving the
three-dimensional hyperbolic grid generation equations consisting of two
orthogonality relations and one cell volume check.

The cell volume check is one of two grid quality checks conducted by
HYPGEN after a grid is generated. The cell volume check is a cell volume
computation using tetrahedron decomposition, and will check the grid for any

types of distortions. The second test is a Jacobian computation and uses a finite volume algorithm, specifically the OVERFLOW flow solvers algorithm [17b]. If a grid passes the two test, it will run through the flow solver. Although, if any cell in the grid passes the second test but not the first test, its accuracy may be effected if those regions.

4.2 Boundary Conditions

The solid wall conditions are specified in CNS as no-slip adiabatic wall. The outer boundary or far field flow variables are set to free stream flow conditions. A symmetry plane is used at the wing's root chord section which eliminates wall effects or the fuselage effect that could lead to leading-edge flow contamination also known as spanwise turbulent contamination. This phenomenon was first discovered by Gray [18] in flight at the Royal Aircraft Establishment (RAE) in 1951.

CHAPTER 5

AUTOMATED STABILITY ANALYSIS

In order to conduct the following parametric study it was necessary to substantially automate the analysis process, due to the extensive amount of man-hours required to obtain a transition prediction. Once this portion of the study was completed it was necessary to validate the Automated Stability Analysis. The F-16xl ship1 Flight test was used as a validation case.

The automated stability analysis is illustrated in Figure 5.1. The actual automation begins after the Pressure coefficients (Cp) are obtained from the mean flow solution for each span station. Once the Cp's are obtained they are fed into the boundary-layer code (WING) which computes the boundary-layer profiles and other parameters. Now the boundary-layer outputs are fed into the Compressible Stability Analysis code (COSAL) to measure the disturbances in the boundary layer. Note that for each span station the stability code must run for a spectrum of frequency between 0 and 40,000 Hz to determine the most unstable condition. The user time required for an average COSAL run is approximately 30 seconds and since the frequency scan requires 22 runs for each of the 8 selected span stations on the wing, a total average time of 1.5 hours. Note that the actual turn around time for a typical job is about 3 hours due to the added time to run the boundary layer code and other post processing codes.

CHAPTER 6

RESULTS AND DISCUSSION

6.1 Stability Automation Validation

Due to the extensive amount of repetitive calculations needed to obtain a transition front solution as mention earlier in Chapter 6, this process was automated and therefore needed to be validated. The validation case used was the F-16XL wing transition front. The results of the F-16XL wing transition front, using this developed automated stability process, compared well with the results previously obtained manually. The advantage of this automated process are that the amount of users interactive man hours has dropped from hours to a matter of minutes, and the overall turn around time for a transition prediction has dropped from days to a matter of hours.

6.2 Reynolds Number Effects

Before a full parametric study was to be conducted, it was necessary to establish a baseline case that had a reasonable region of laminar flow. This was necessary so that the effects of changing the various parameters could be distinguished. To obtain a fair amount of laminar flow and maintain the supersonic cruise conditions of a free stream mach number equal to 1.5 and an altitude of 40 to 50 thousand feet, the Reynolds number was varied by changing the root chord length. The results showed that the extent of laminar flow was increased as the local Reynolds number was decreased. A root chord of 5 feet was selected for the Baseline case and yields laminar flow up to approximately 20% chord figure 6.1.

6.3 Angle of Attack Effects

Effects of angle of attack study on the extent of laminar flow has shown that Laminar flow is increased with increase angle of attacks. This is illustrated in figure 6.2 by the Transition fronts of the Baseline, 45 degree swept, wing for angle of attacks of 0, 5, and 10 degrees. The white region signifies the portion of the wing where laminar flow is no longer predicted. The color contours represent the measure of the disturbance levels (N-factors) in the Boundary Layer and range from 0 to 10. The disturbance level of 8 was selected as the critical transition N-factor based on previous swept wing studies [3]. It should be noted that the transition results near the tip and root of the wing are not valid as mentioned earlier, due to the conical flow assumption in the boundary-layer program which are fed into the transition predicting Compressible boundary-layer Stability code (COSAL). To avoid the tip and root regions of the wing, the analysis was only performed on the grey area shown in figure 6.3. Furthermore, to simplify the discussion of the results, only the mid span of the wing will be mentioned in detail.

In order to understand the transition results, a flow trace of the different angle of attack cases is shown in figure 6.4. These flow traces reveal a decrease in crossflow near the leading edge of the wing as the angle of attack increases to 10 degrees. In order to better see how the flow trace is affected by the different angle of attacks, a plot of the leading edge flow at 48% span is shown in figure 6.5. It should be noted that the black line indicates the leading edge and the 48% span is on the right hand side. The green flow trace line indicates the flow trace at the leading edge point. The red flow trace lines indicate the flow over the upper wing surface and the blue indicate the flow trace on the lower wing surface. From this plot it is evident that the attachment point moves below the leading edge on to the lower surface of the wing.

From a previous parametric study on the leading edge attachment line of

the F-16XL [16] it was found that the maximum crossflow velocity at a given wing location decreased as the angle of attack increased due to the rotation of the attachment point underneath the leading edge. Although, the results of this study reveal a different trend and are shown in the following boundary-layer profile results. Unlike the expected upstream movement of transition as mentioned in the F-16XL attachment line study, the transition results of this study show that transition moves downstream (figure 6.2).

In order to study the flow more thoroughly, boundary-layer profile plots were made for the three angle of attack cases at approximately mid span (48% span). Since transition is found to occur at an x/c between 10 and 21%, crossflow boundary-layer profiles were plotted from x/c of 0 to 21% as shown in figure 6.6. Results of the crossflow profiles reveal that the crossflow velocities are larger for the higher angle of attack cases near the leading edge and then it is found that the higher angle of attack case's crossflow damp fall below the lower angle of attack case farther down stream. In order to represent this trend a plot of the maximum crossflow for the first 21% chord at the different angle of attacks is shown in figure 6.7. This figure is a plot of the maximum crossflow "$(W/Uinf)max$" versus streamwise location "X/C" for the angle of attacks of 0, 5, and 10 degrees. This plot shows that the maximum crossflows are larger as the angle of attack is increased to approximately 4% chord. After 4% the crossflows for the 5 degree angle of attack case fall below the 0 angle of attack case and level off at approximately -0.045 after 15% chord. The 0 angle of attack case slowly falls after 4% chord and levels off at approximately -0.06. The 10 degree angle of attack case falls below the 0 degree angle of attack case at approximately 8% chord and continues to fall below the 5 degree angle of attack case at approximately 15% chord and appears to begin leveling off at 21% chord at a crossflow value of 0.04.

Streamwise boundary-layer profiles were also plotted (figure 6.8). The results of the streamwise boundary profiles show that the velocity components in the streamwise direction increase significantly as the angle of attack increases for any given x/c values up to 21 percent. This is attributed to the increase streamwise curvature that the flow experiences, which requires the flow over the top of the wing to increase its streamwise velocity component to account for the pressure differences across the wing. It should be noted that the streamwise component of the velocity profiles are not considered in the stability of the boundary-layer since they influence the Tollmein Schilichting instabilities and the current calculation is for crossflow instabilities.

Next, Stability curves of the transition results at approximately 48% Span, are shown in figure 6.9. This figure is a plot of x/c vs. frequency for the angle of attack study at a the critical boundary-layer disturbance level (N-factor) of 8. Basically, this plot shows the most unstable frequencies that yield the disturbance levels of 8, and where these disturbances first occur. For example, at the angle of attack case of 0 degrees, the curve indicates that the most unstable frequencies which yields the earliest transition is approximately 14000 Hz and occurs at the x/c value of approximately 12 percent. Therefore, it is revealed that the transition front moves back as the wing's angle of attack is increased to 10 degrees. It should also be noted that the critical frequency at which transition is predicted in both the 0 and 10 degree case is approximately 14000 Hz, and for the angle of attack case of 5 degrees it is approximately 12000 Hz which means that the disturbance in the flow are higher for a lower disturbance frequency for the 5 degree angle of attack case.

6.4 Sweep Effects

In addition to investigating the effects of angle of attack, the effects of sweep were also studied. It was necessary to keep the wing's aspect ratio constant so that the comparison in sweep would not be misinterpreted by other changes in the wing's surface area or local chord. It was also necessary to avoid sweeping the wing into the mach cone, which would cause shock waves and distort the flow. Due to the above requirements, it was necessary to shear the baseline clipped delta wing to obtain the different sweeps and maintain the same aspect ratio as well as local chord lengths. To obtain sweeps of 45 degrees to 70 degrees, three new geometries were created as shown in figure 6.10. This led to two sets of sweep comparisons. The first set compared the 45 and 60 degree sweeps with aspect ratio's of 1.45. The second set compared the 60 and 70 degree sweeps with an aspect ratio's of 1.0. The lower AR wings of 1.0 were created to allow the analysis of the 70 degree swept wing, which would avoid sweeping into a shock wave created by the mach cone at the freestream mach number of 1.5.

The first set of sweep transition front results compare the 45 and the 60 degree sweeps at an AR of 1.45 and are shown in figure 6.11. It should be noted that all sweep comparisons were conducted at an angle of attack of 0 degrees. The results of this first set show that the transition in the center of the wing occurs earlier for the 60 degree sweep then the 45 degree sweep and substantially earlier near the wing tip. From the flow traces shown in figure 6.12, it is apparent that the 60 degree swept wing experiences a larger crossflow near the leading edge of the wing. It should also be noted that the 60 degree swept wing appears to have a flow separation occurring near the tip trailing edge of the wing.

Again the analysis of the 48% span is used to show a more detail comparison. The results of the crossflow profiles (figure 6.13) show that as the

wing is swept back to 60 degrees, the crossflow is substantially increased for all streamwise station up to 20 percent chord. In order to represent this trend a plot of the maximum crossflow for the first 21% chord at the different angle of attacks is shown in figure 6.14. This figure is a plot of the maximum crossflow "(W/Uinf)max" versus streamwise location "X/C" for the for the first set of sweeps. This plot shows that the maximum crossflow is at first slightly larger for the 45 degree sweep at 1% chord and then drop below the 60 degree sweep at 3% chord. The max crossflow for the 45 degree case then levels off at about 0.06 W/Uinf after approximately 15% chord. The 60 degree sweep's maximum crossflow velocities are larger after 2% chord and continue a small fluctuation at a value of about 0.07 W/Uinf after 10% chord.

The results of the streamwise flow profiles (figure 6.15) show that the streamwise velocity component for the 60 degree sweep maintains about a 5% larger edge velocity. Although, within the boundary layer the profile are similar. As noted earlier the streamwise velocities are not used in the boundary-layer stability analysis and from the results are indeed not a crucial part of the transition affects due to sweep.

Next, Stability curves of the transition results for the first set of sweep analysis at 48% span are shown in figure 6.16. This is the same type of plot as the one discussed in the angle of attack study earlier. The results show that transition occurs at approximately an x/c of 12 percent and frequency of 14,000 Hz for the 45 degree sweep. For the 60 degree sweep transition occurs at an x/c of approximately 10 percent and frequency of approximately 20,000 Hz. Therefore, transition is move forward two percent chord when the wing is swept from 45 to 60 degrees.

The transition results of the second sweep comparison show a delay in the transition front as the wing is swept from 60 to 70 degrees (figure 6.17). As was

expected for the higher swept case there exists a larger crossflow, as shown in the flow trace of figure 6.18. Furthermore, the flow trace of the 70 swept wing indicates that a flow separation may be occurring near the trailing edge tip section of the wing. Unlike the previous 60 degree swept wing were the separation occurred across the wing tip (figure 6.14), the separation of the 70 degree swept wing seems to move away from the wing tip and contaminate more of the wing as shown in figure 6.18.

Comparison of the 48% span transition trends and boundary layer profiles of this second sweep comparison will now be discussed. The crossflow velocity profiles show that the 70 degree swept case contains higher crossflow velocities then the 60 degree swept geometries (figure 6.19) after 5 percent chord. The maximum crossflow for each streamwise station (figure 6.20) show that initially the 60 degree sweep case are larger for the first 5 percent chord, yet they are decreasing while the 70 degree sweep case maximum crossflow are increasing. After 5 percent chord the 60 degree sweep case continues to decease its maximum crossflow velocities until it reaches a average value of about -0.065 between 15 and 21 percent chord. The 70 degree case continues to increase to a value of about -.085 at 21 percent chord. The streamwise velocity profiles (figure 6.21) show that no significant change occurs as the wing is swept back to 70 degrees.

Finally, the results of the stability curve for this second set of sweeps at 48% span are shown in figure 6.22. These results (figure 6.22) show that transition occurs at approximately an x/c of 13 percent and frequency of 18,000 Hz for the 60 degree sweep. For the 70 degree sweep transition occurs at an x/c of approximately 25 percent and frequency of approximately 14,000 Hz. Therefore, transition is move back about 12 percent chord when the wing is swept from 60 to 70 degrees.

6.4 Grid Refinement

Now that the above results have been obtained, it was necessary to validate that the result were grid independent. This required making sure that the results did not change with increased grid resolution. Results of this portion of the study are not yet obtained. This effort is on going.

CHAPTER 7

CONCLUSIONS

In the future, a leading-edge shape study will be conducted in the hopes of finding the effects of bluntness at supersonic speeds with respect to the extent of laminar flow.

The result of the angle of attack study revealed that the amount of laminar flow is increased as the angle of attack is increased. These results are not yet understood and are be studied further.

The results of the first set of sweeps, 45 to 60 degrees, show that transition occurs earlier as the wing is swept back, therefore decreasing the amount of laminar flow due to the higher crossflows.

The results of the second set of sweeps at 48% span reveal that the transition is actually delayed therefore increasing the amount of laminar flow by twice the amount rather then decreasing the amount of laminar flow as would be expected due to the higher crossflows at the higher sweep. These result is not yet know and is be studied.

Finally, investigation of the numerical methods being applied in this study have led to the following recommendations. It was found that the two dimensional boundary layer code uses a conical flow assumption that is not truly valid for swept wings and should be replaced with a three dimensional boundary layer code. Furthermore, it is recommended that future research directly use Navier Stokes in place of the Boundary Layer solutions.

REFERENCES

1. Mujeeb R. Malik, High Technology Corporation, Hampton, Virginia,
    "Stability Theory for Laminar Flow Control Design", Progress in
    Astronautics and Aeronautics, Vol 123 1990, pp. 3-46.

2. Morkovin, M.V., "Critical Evaluation of Transition from Laminar to
    Turbulent Shear Layer with Emphasis on Hypersonically Traveling
    Bodies", AFFDL-TR-68-149 (available as NTIS AD-686178), 1969.

3. D. M. Bushnell & M.H. Tuttle, "Survey and Bibliography on
    Attainment of Laminar Flow Control in Air Using Pressure Gradient
    and Suction", NASA RP 1035, Vol I., September 1979.

4. A. J. Srokowski, "Mass Flow Requirement for LFC Wing Design", AIAA
    Paper 77-1222, Aug. 1977.

5. Kosin, R. E.: Laminar Flow Control by Suction as Applied to the
    X-21 Airplane, Journal of Aircraft, Vol 2, September-October 1965,
    pp. 384-390.

6. Fischer, Michael C.; and Ash, Robert L.: A General Review of
    Concepts for Reducing Skin Friction, Including Recommendations for
    Future Studies TM X-2894, March 1974, NASA.

7. Beckwith, I.E., "Development of High Reynolds Number Quiet Tunnel
    for Transition Research", AIAA Journal, Vol 13, No. 3, March 1975,
    pp. 300 to 306.

8. Pfenninger, W., "USAF and Navy Sponsored Northrop LFC Research
    Between 1949 and 1967", in "Workshop on Laminar Flow Control",
    compiled by C. T. D'Aiutolo, NASA Langley Research Center,
    April 6-7, 1976, pp. 14-50.

9. Unver Kaynak, Terry L. Holst, and Brian J. Cantwell, "Computational
    of Transonic Separated Wing Flow Using an Euler/Navier-Stokes Zonal
    Approach", NASA Technical Memorandum 88311.

10. Kalle Kaups and Tuncer Cebeci, Douglas Aircraft Company, Long Beach Calif, "Compressible Laminar Boundary Layers with Suction on Swept and Tapered Wings", Journal of Aircraft, Vol 14, No.7, July 1977, pp. 661-667.

11. Mujeeb R. Malik, "COSAL: A Black-Box Compressible Stability Analysis Code for Transition Prediction in Three-Dimensional Boundary Layers", High Technology Corp., NASA Contractor Report 165925, 1982.

12. Beam, R. and Warming, R.F., "An Implicit Finite-Difference Algorithm for Hyperbolic Systems in Conservation-Law Form," Journal of Comp. Physics, Vol.22, Sept. 1976, pp. 87-110.

13. Pulliam, T. H., "Euler and Thin-Layer Navier Stokes Codes: ARC2D, and ARC3D," Notes for the Computational Fluid Dynamics Users' Workshop, The University of Tennessee Space Institute, Tullahoma, Tenn., Mar. 12-16, 1984.

14. Chan, W.M. and Steger, J.L., "A Generalized Scheme For Three-Dimensional Hyperbolic Grid Generation", AIAA Paper 91-1588, Proceedings of the AIAA 10th Computational Fluid Dynamics Conference, Honolulu, Hawaii. 1991.

15. Charles L. Ladson and Cuyler W. Brooks, Jr., NASA Langley Research Center: "Development of a Computer Program to Obtain Ordinates For NACA6- and 6A- series Airfoils", June 25, 1974.

16. Flores, J., Tu E.L., Anderson B., and Landers, S., "A Parametric Study

of the Leading Edge Attachment Line for the F-16XL", AIAA Paper 91-1621, Proceedings of the AIAA 22nd Fluid Dynamics, Plasma Dynamics & Laser Conference, Honolulu, Hawaii. June 24-26, 1991.

Transition
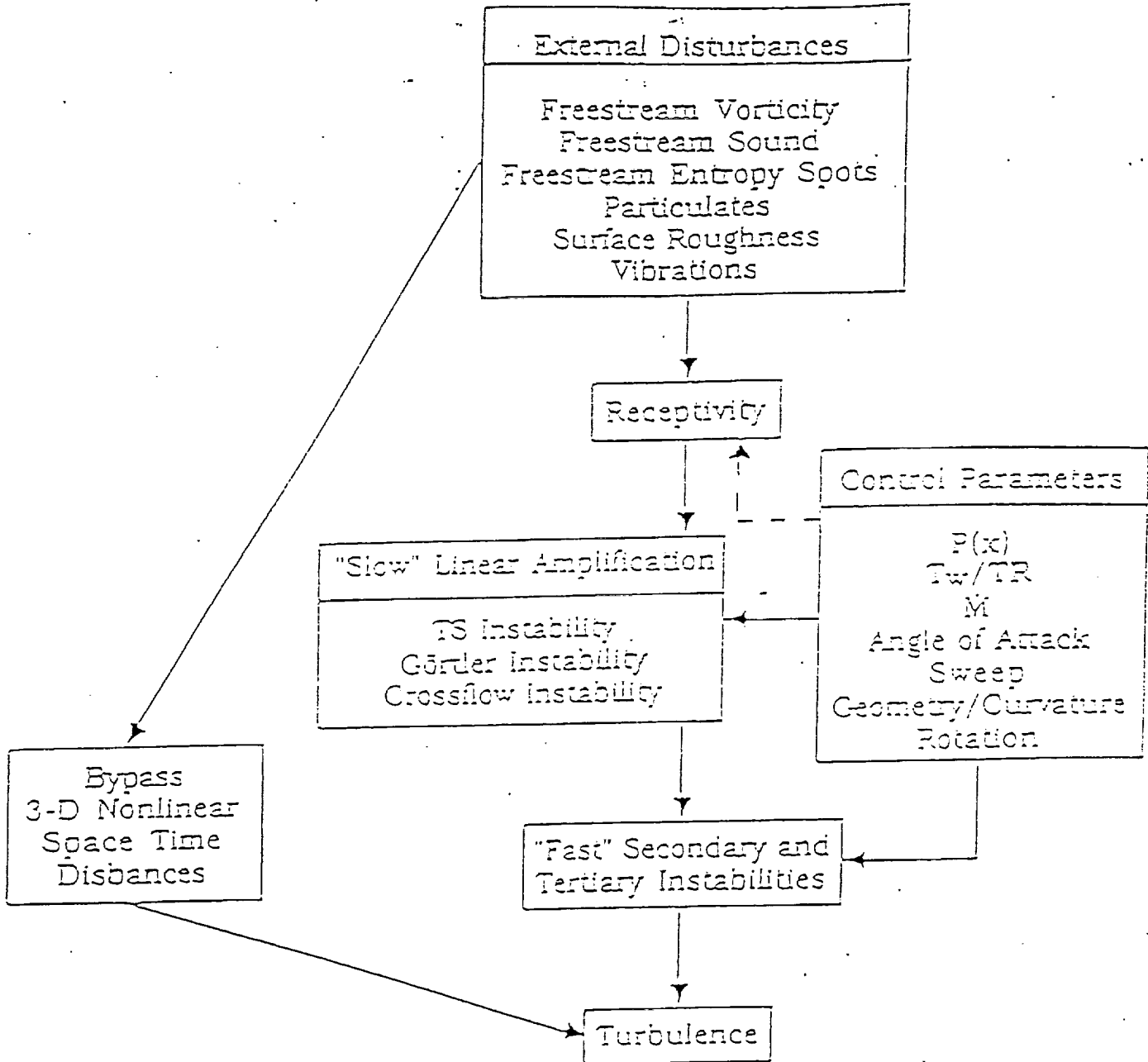
FIG. 1.1 Transition Flow chart
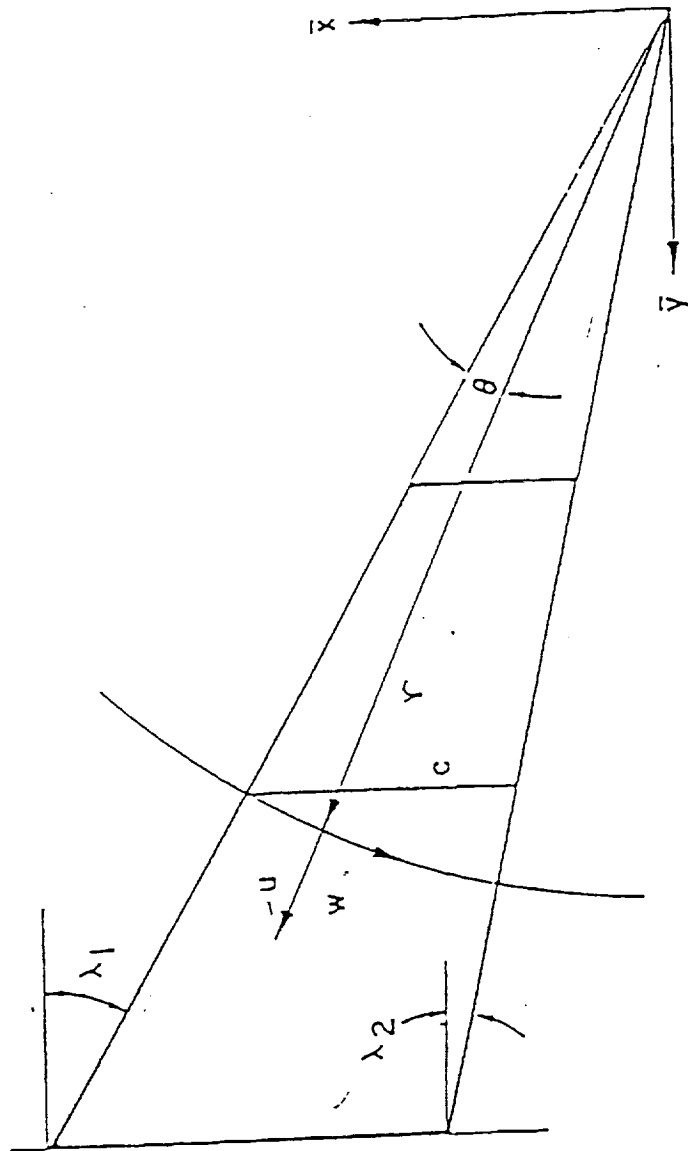
Tapered wing and the polar coordinate system.

Fig. 2.1

AUTOMATED STABILITY ANALYSIS
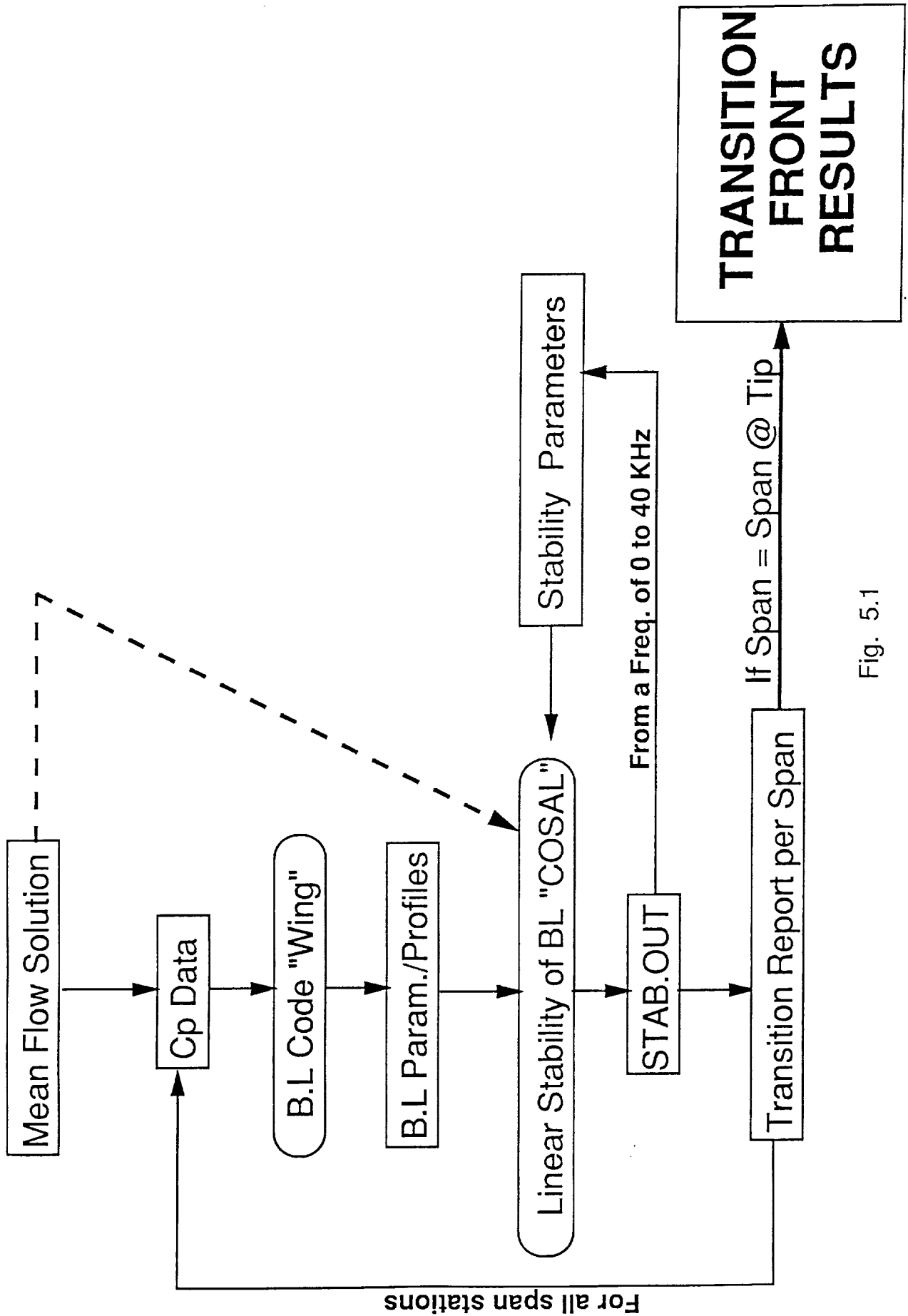
Fig. 5.1

Baseline Case Transition Front [Alpha = 0 deg.]

N-fact criteria = 0.0   Date: Sep 25, 1992

MACH   1.500
ALPHA   0.00 DEG
Re   6.3x10**6
Xo   49xR
GRID

CONTOUR LEVELS
0.00000
1.00000
2.00000
3.00000

5.00000
6.00000
7.00000
8.00000
9.00000
10.00000
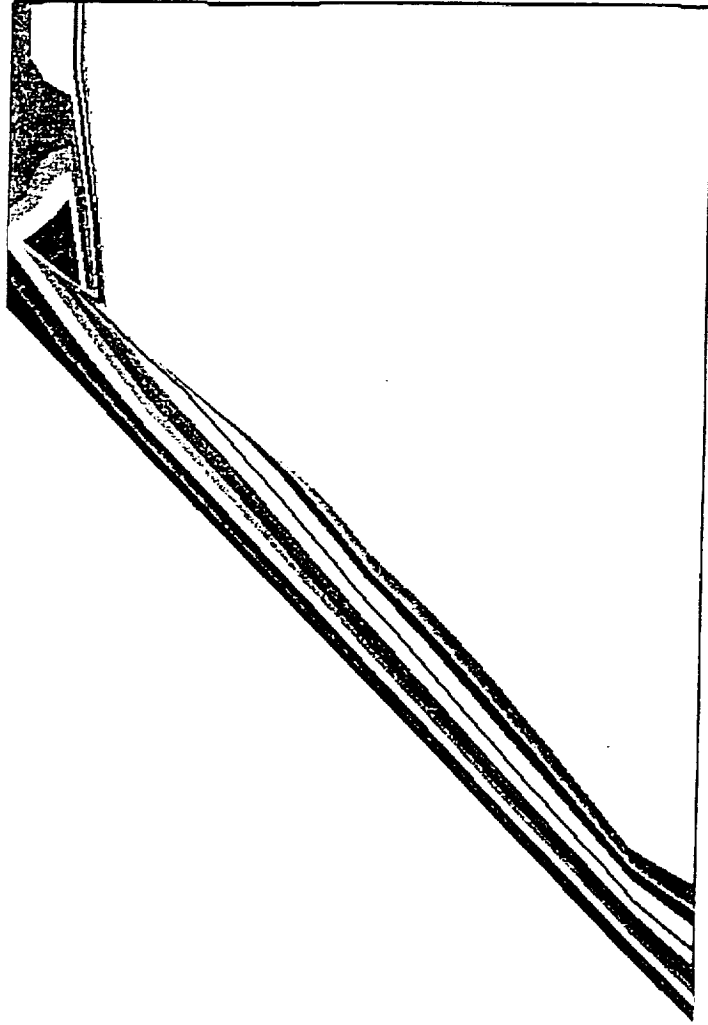
Fig. 6.1 Transition Front

Transition Front's Angle of Attack Effects .
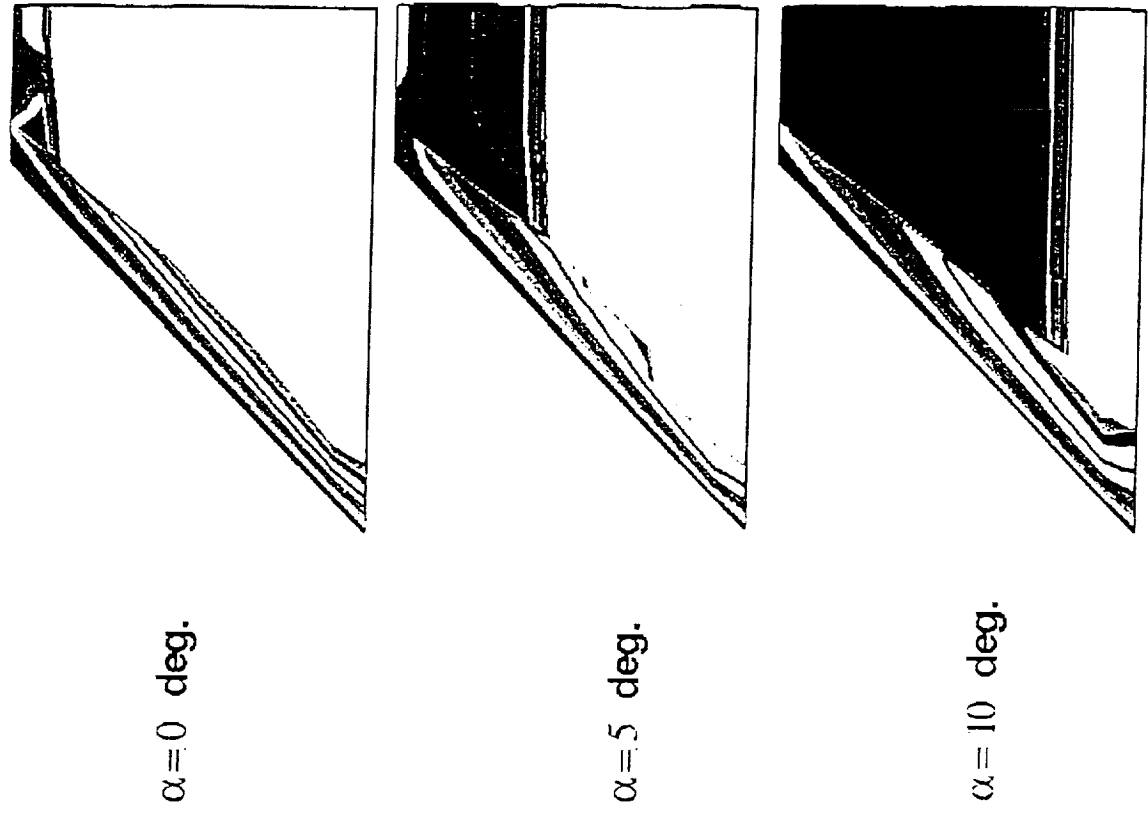
$\alpha = 0$ deg.

$\alpha = 5$ deg.

$\alpha = 10$ deg.

CONTOUR LEVELS
0.00000
1.00000
2.00000
3.00000

5.00000
6.00000
7.00000
8.00000
9.00000
10.00000

Fig 6.2 Transition Front Angle of Attack effects on the Baseline 45 degree swept wing
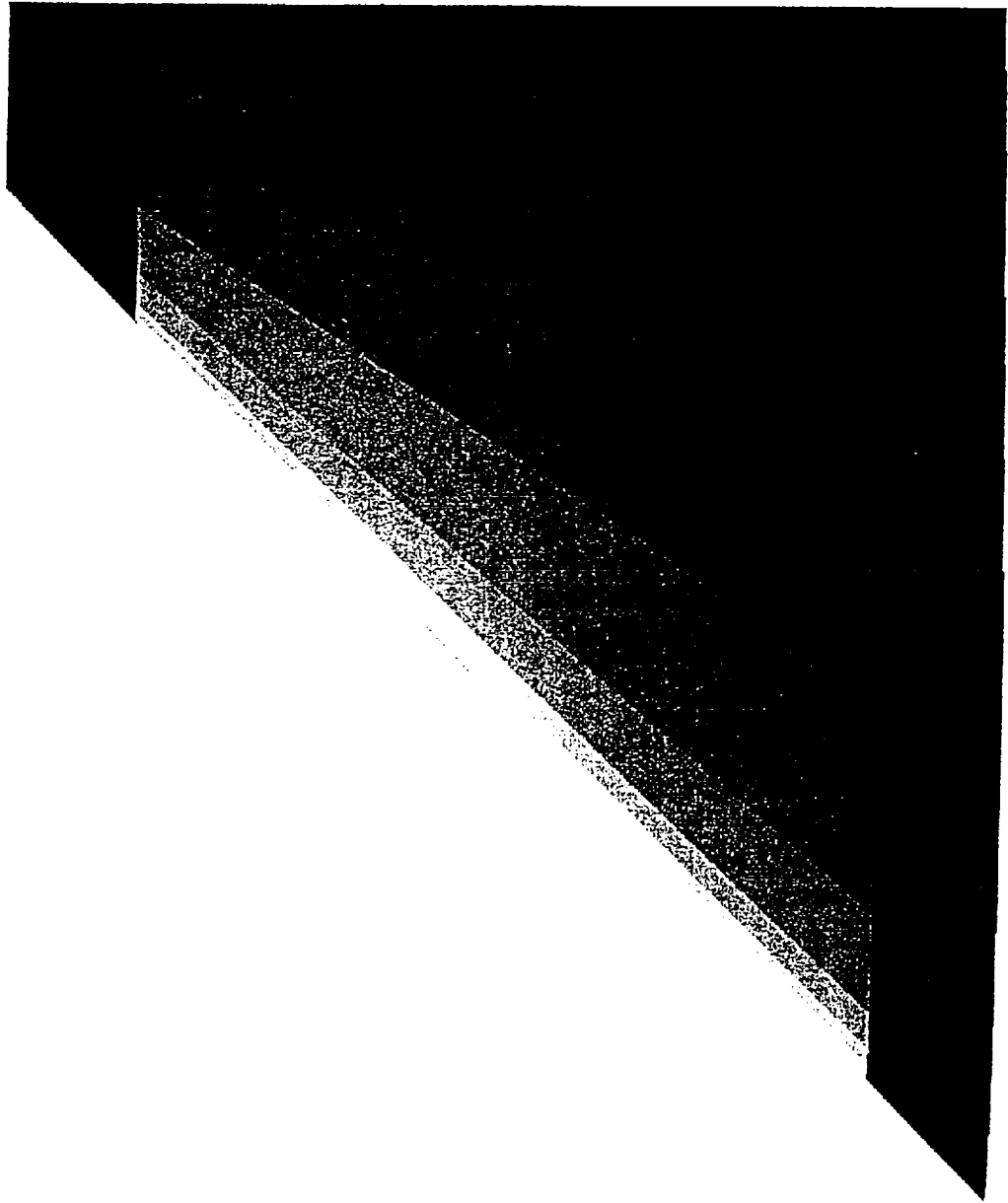
Fig 6.3 Boundary-layer stability analysis region

45WING Flow Trace Comparison

Case1 (Baseline)
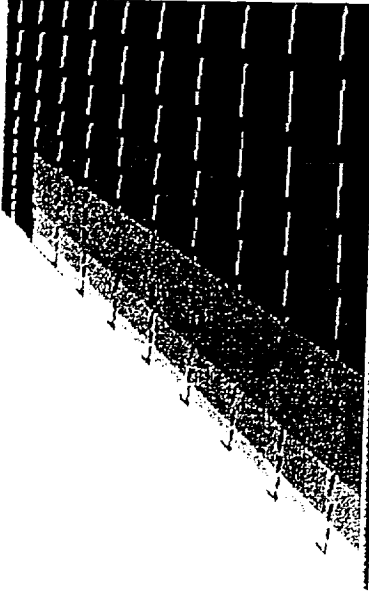
$\alpha = 0$ deg.

Case 2
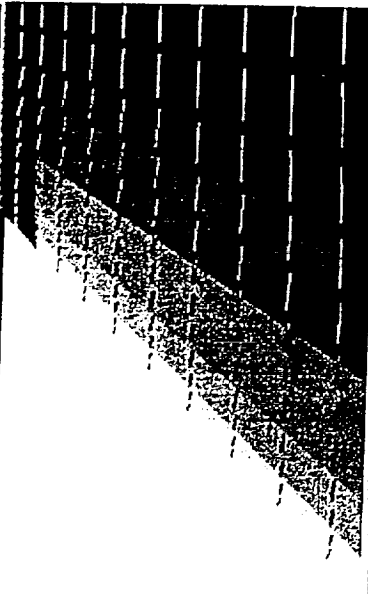
$\alpha = 5$ deg.

Case 3
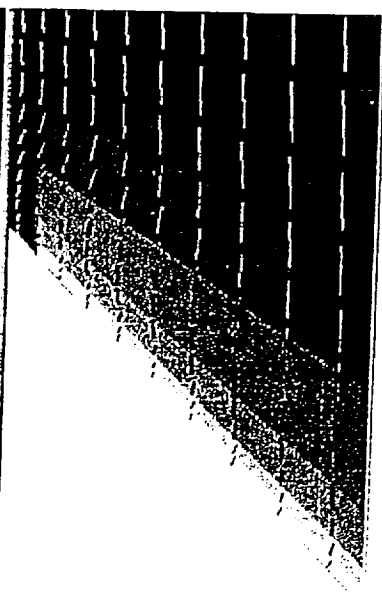
$\alpha = 10$ deg.

Fig 6.4 Flow Trace

Leading Edge Flow Trace

45WING BASELINE CASE 1

Angle of Attack = 0 deg.

45WING CASE 2

Angle of Attack = 5 deg.

45WING CASE 3

Angle of Attack = 10 deg.
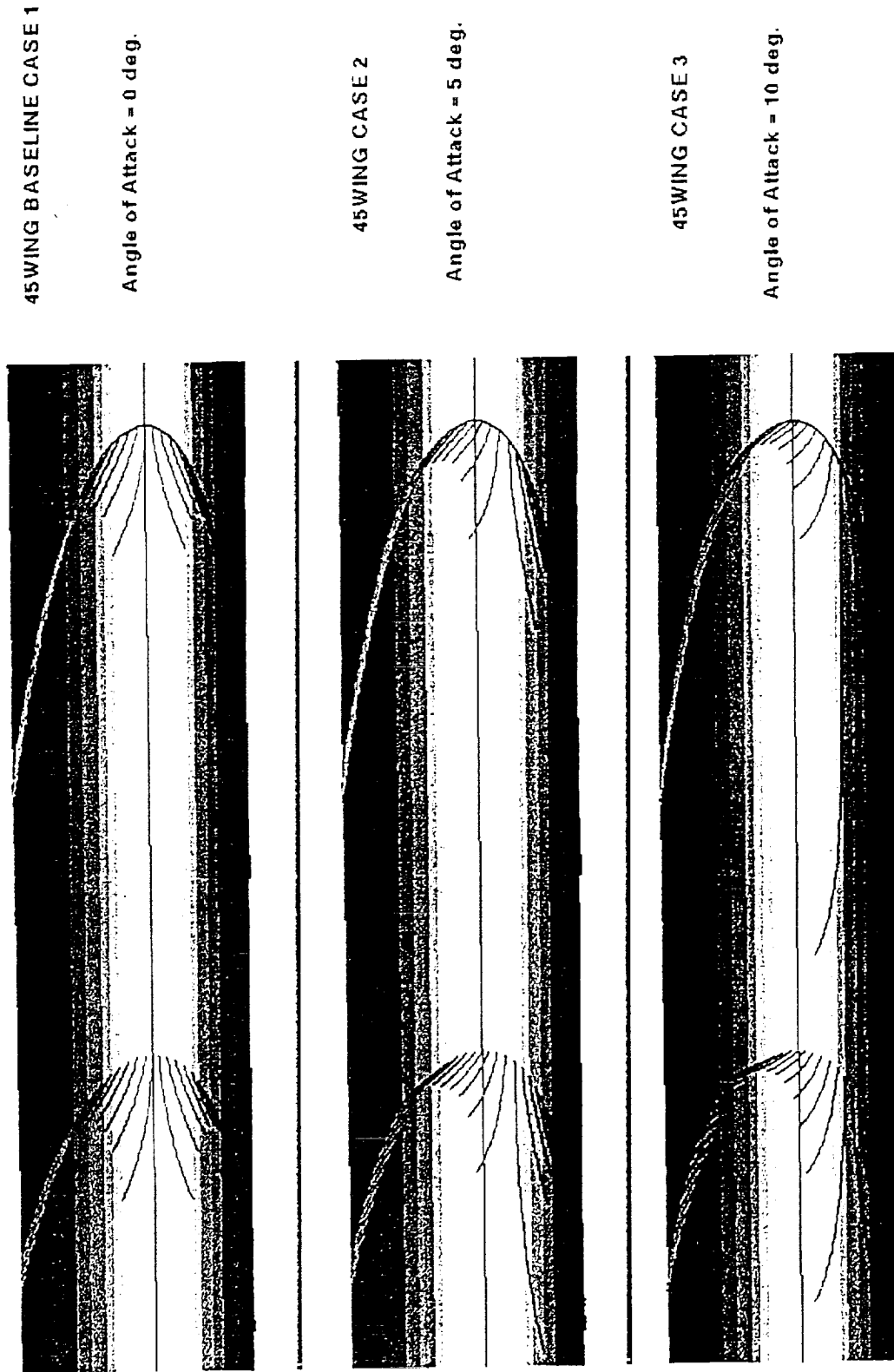
Fig. 6.5   Flow trace patterns about the leading edge @ 48% Span for angles of attack of 0, 5, and 10 degrees.

Cross Flow Boundary Layer Profile @ 48% Span
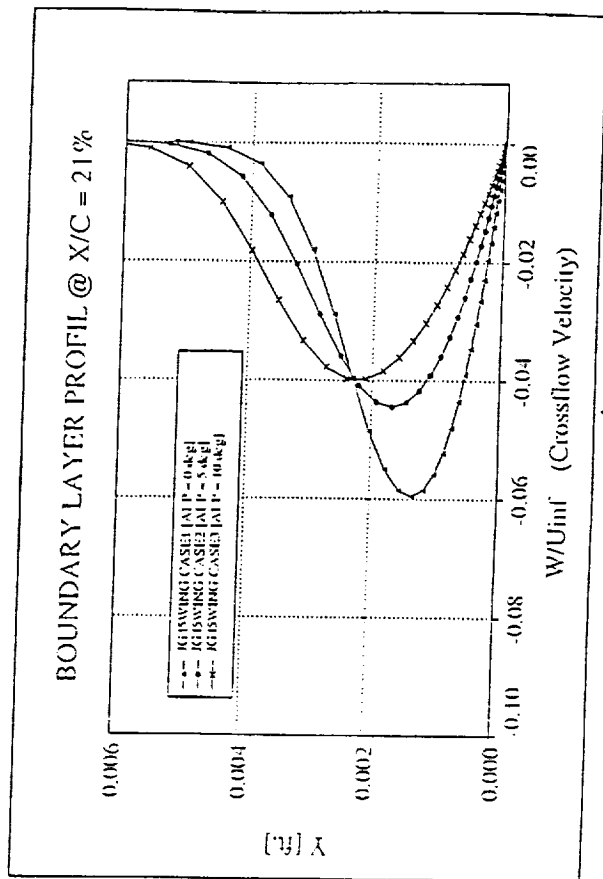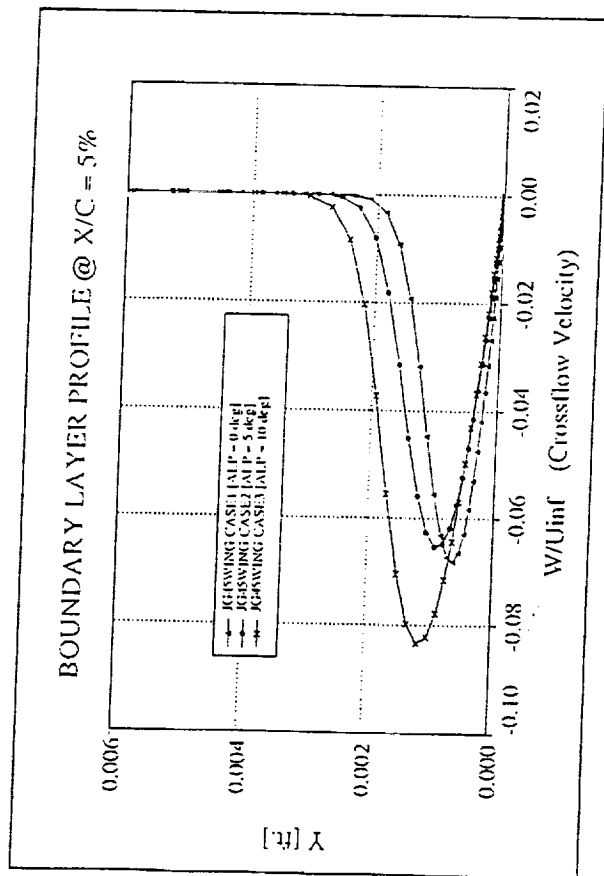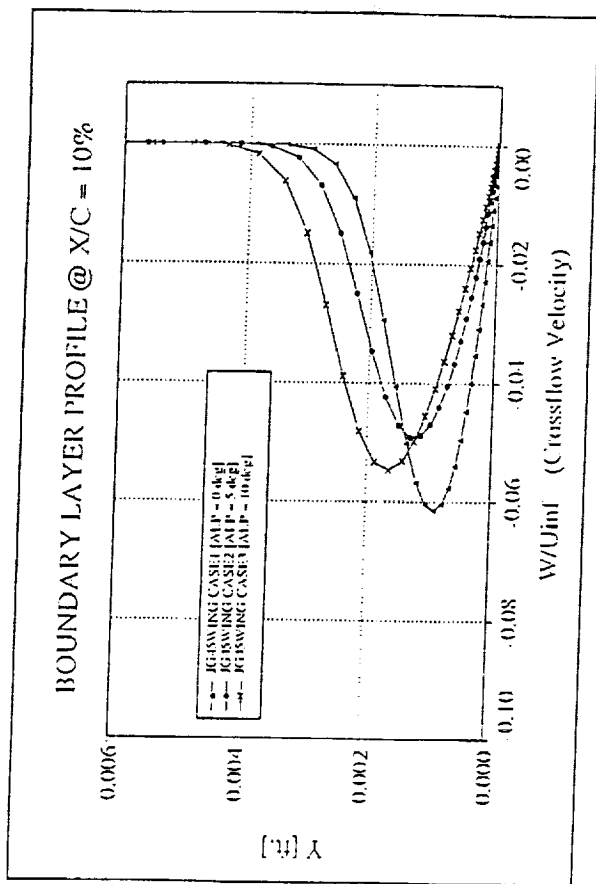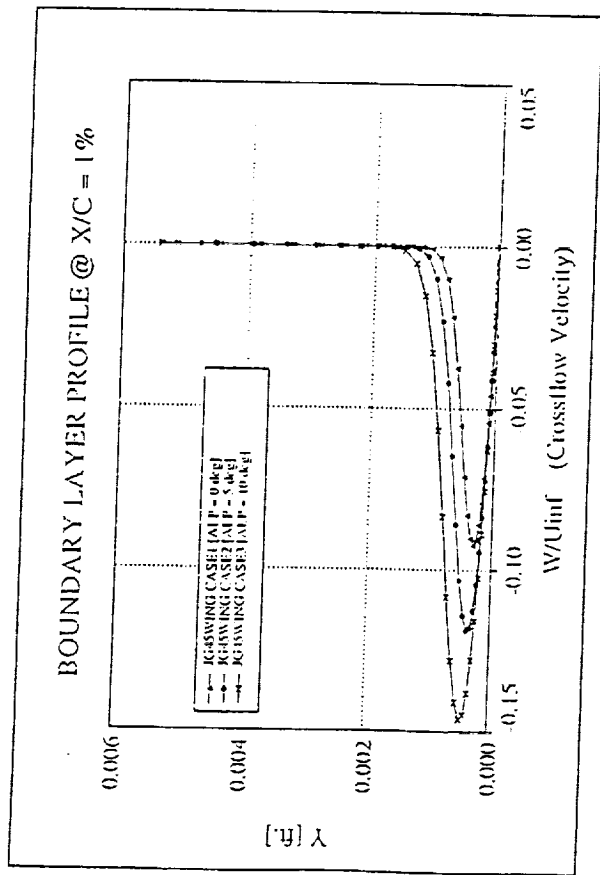
FIG. 6.6 Cross Flow Profile change with α @ 48% Span for various airfoil stations.

Maximum Crossflow Effect Due to AOA at 48% Span

Legend:
- 45WING CASE1 [AOA = 0 deg]
- 45WING CASE2 [AOA = 5 deg]
- 45WING CASE3 [AOA = 10 deg]

X/C

W/Uinf max
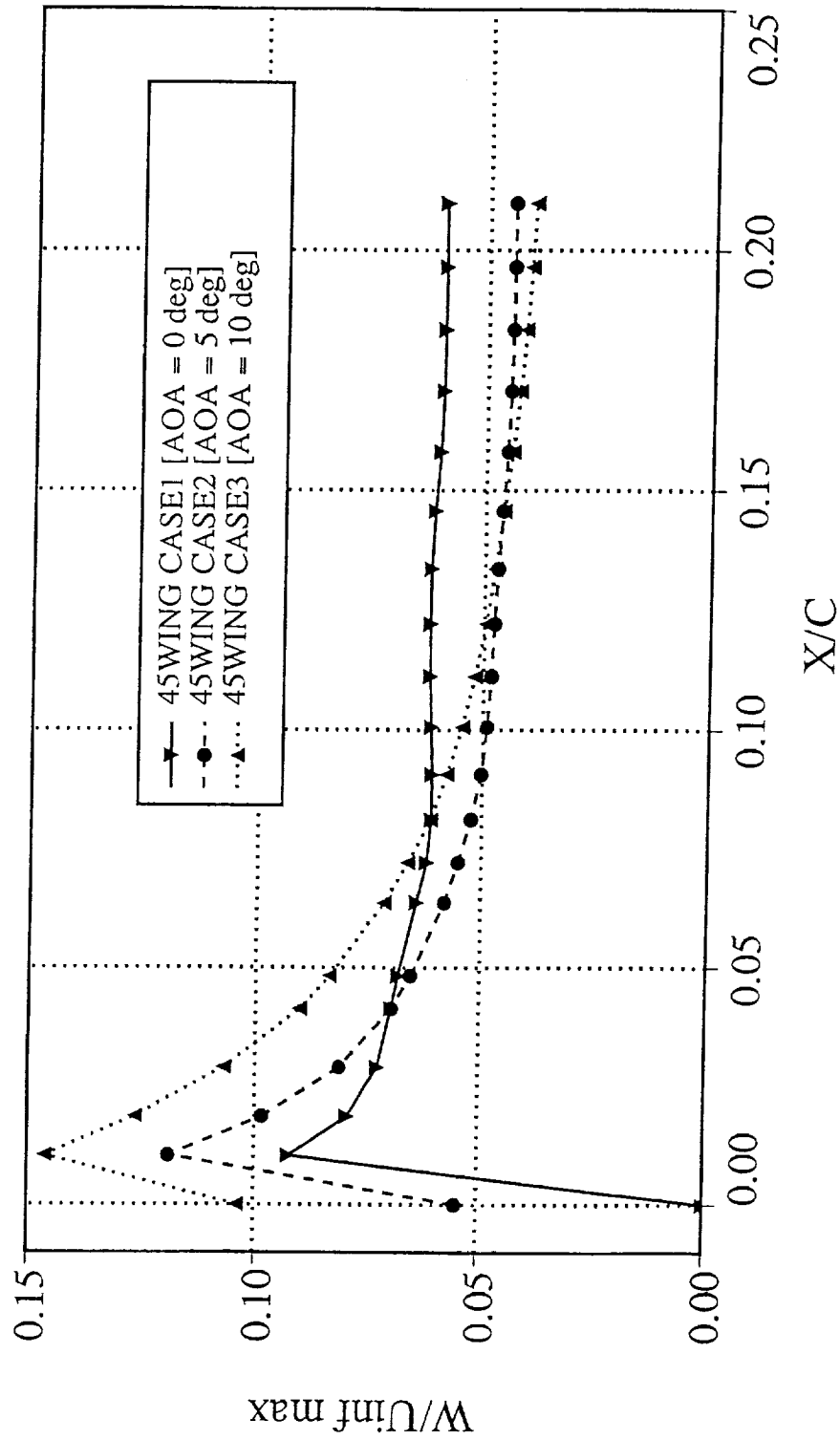
Fig. 6.7

Streamwise Boundary Layer Profile @ 48% Span
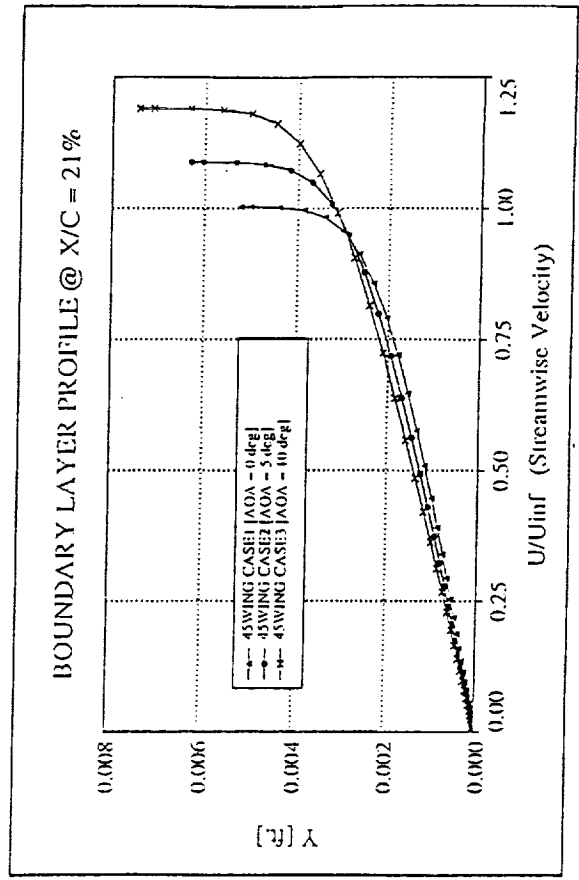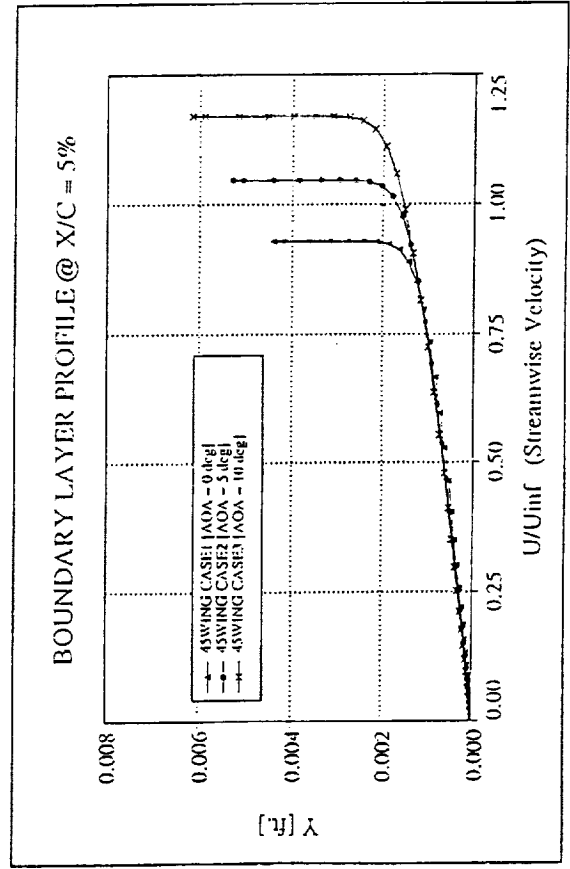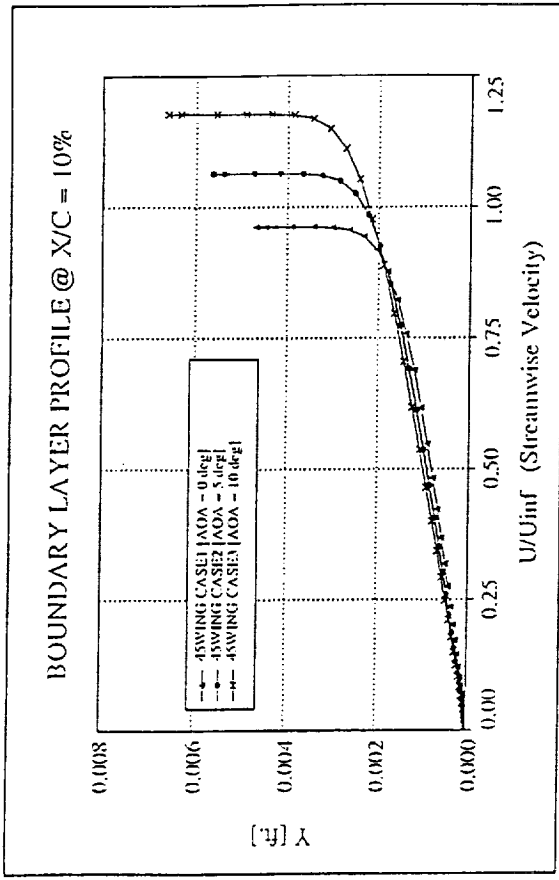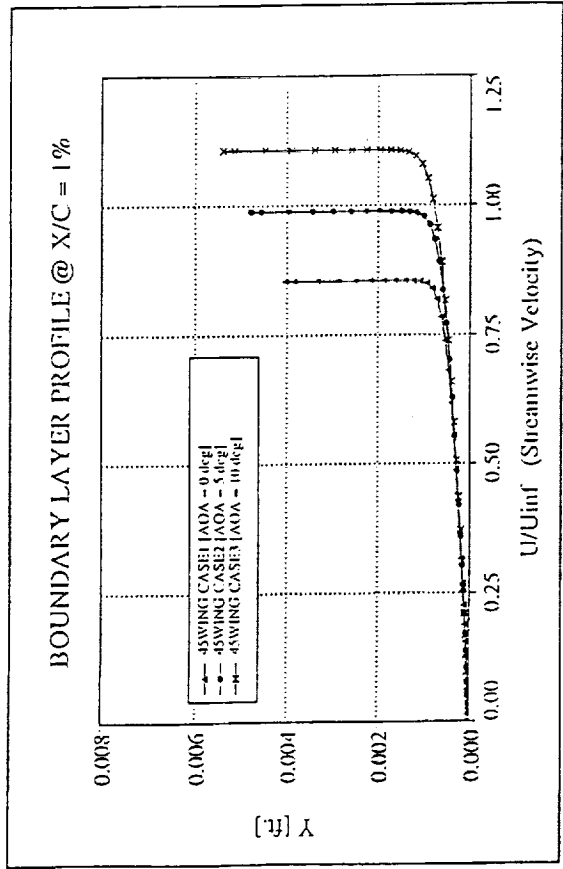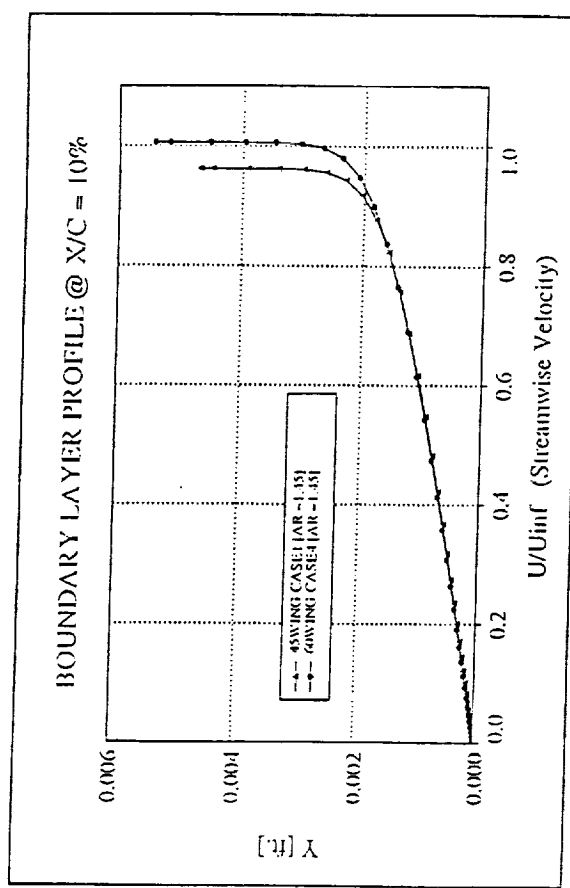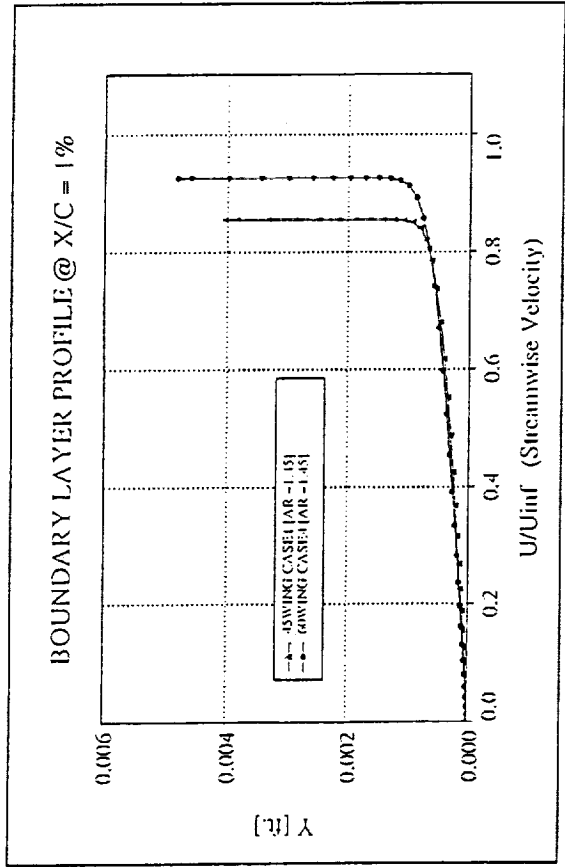

FIG. 6.8 Streamwise Flow Profile change with α @ 48% Span for various airfoil stations.

Stability Curve Transition Results @ 48% Span
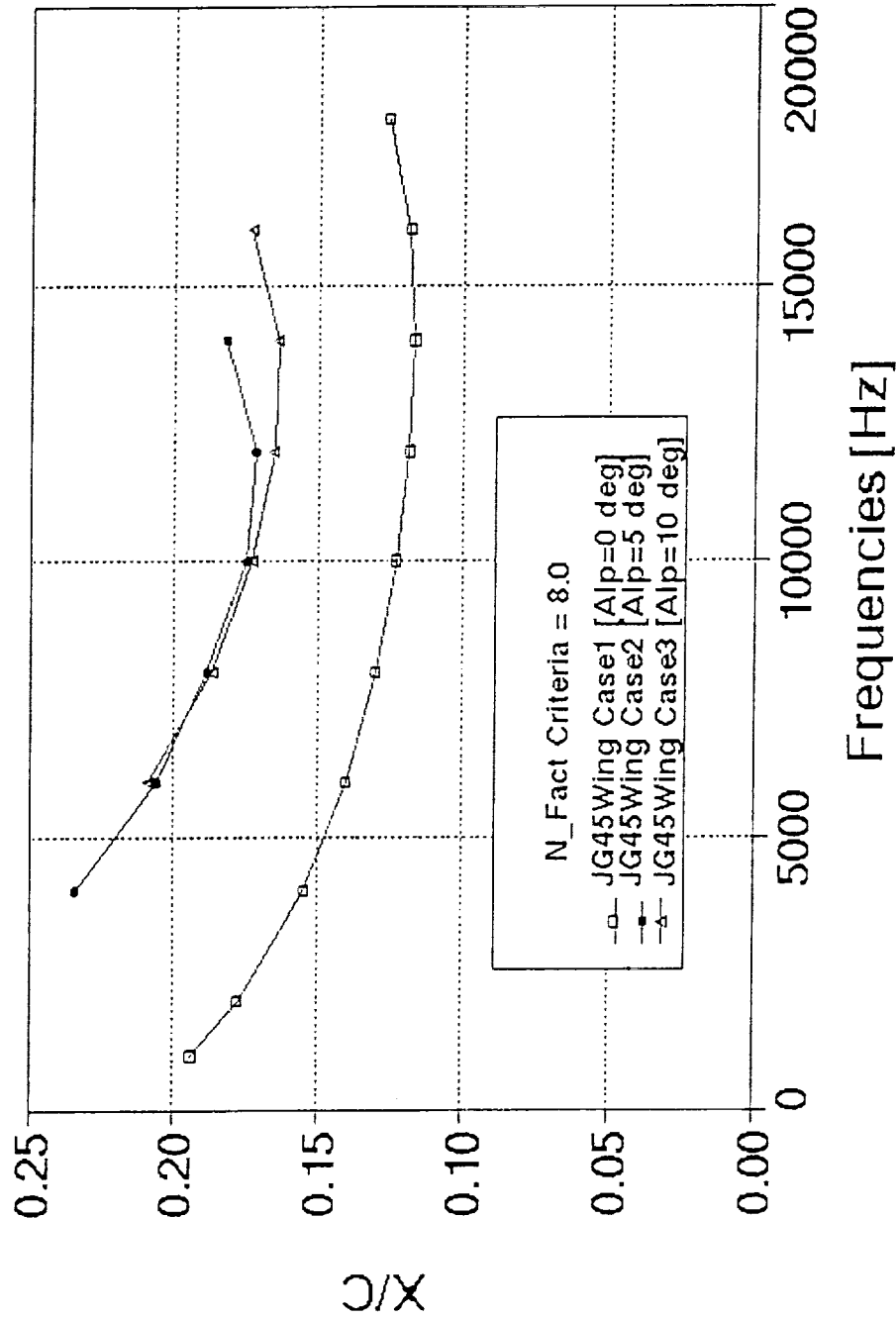
N_Fact Criteria = 8.0
—▼— JG45Wing Case1 [Alp=0 deg]
--●-- JG45Wing Case2 [Alp=5 deg]
·····▲···· JG45Wing Case3 [Alp=10 deg]

X/C

Frequencies [Hz]

Fig. 6.9

Fig 6.9 Transition Stability Curves

New Swept Geometries

60Wing1

Aspect Ratio = 1.45

Leading Edge Sweep = 60 deg.

Trailing Edge Sweep = 36.2 deg.

60Wing2

Aspect Ratio = 1.0

Leading Edge Sweep = 60 deg.

Trailing Edge Sweep = 5.5 deg.

70Wing

Aspect Ratio = 1.0
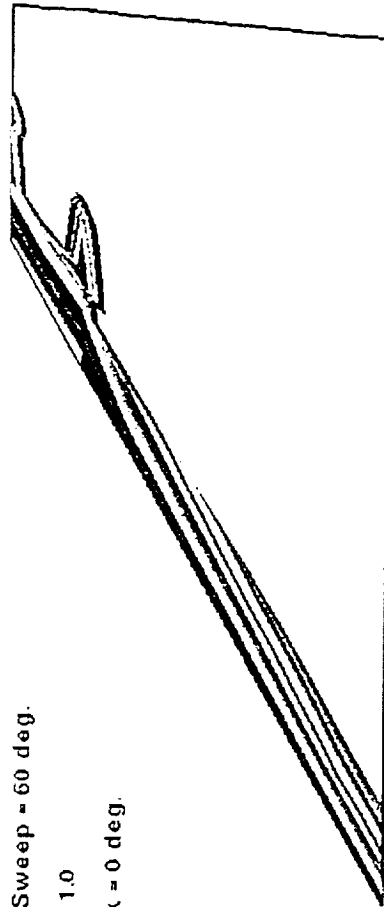
Leading Edge Sweep = 70 deg.

Trailing Edge Sweep = 48.01 deg.
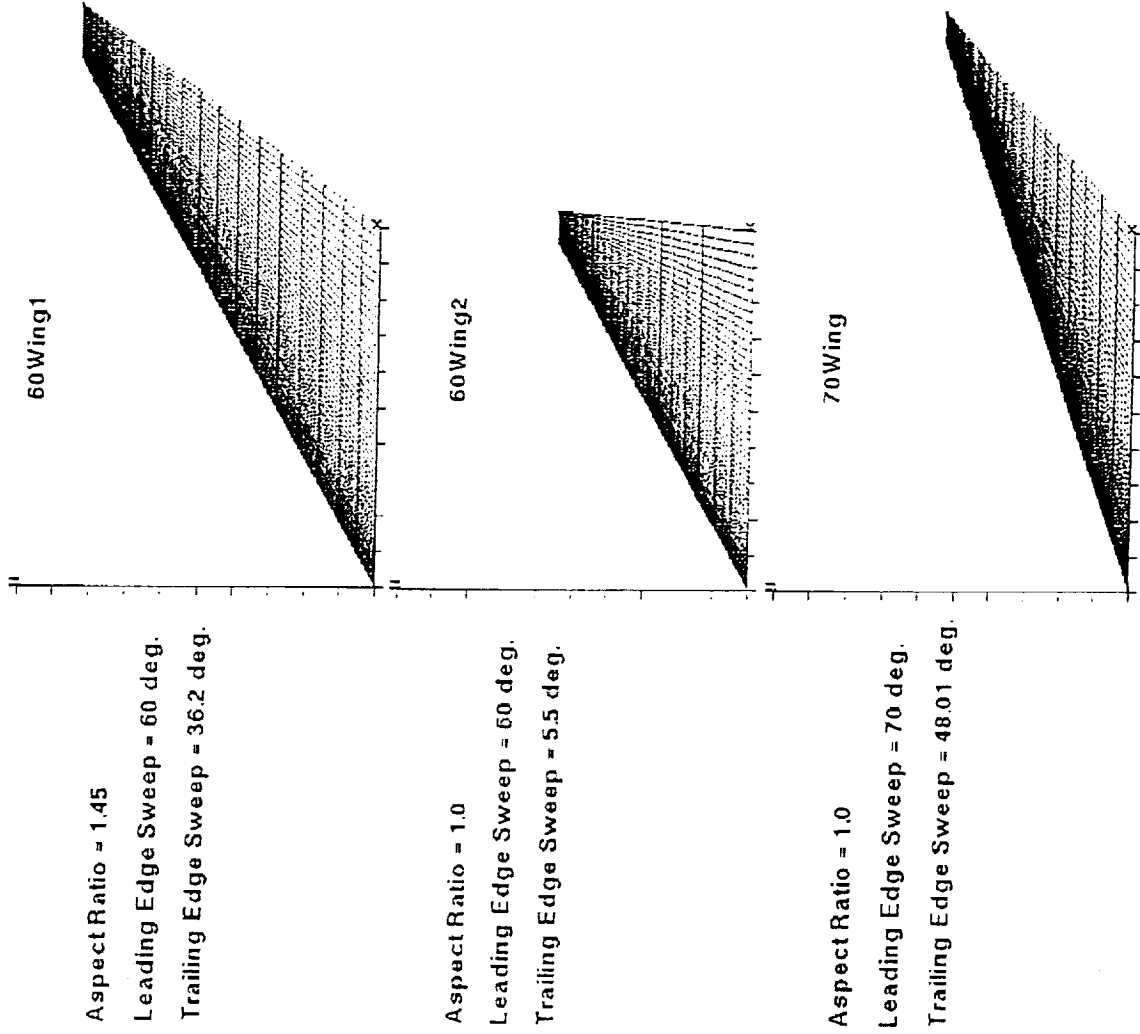
Fig. 6.10

Transition Front Sweep Effects [Set 1]

Leading Edge Sweep = 45 deg.

Aspect Ratio = 1.45

Angle of Attack = 0 deg.

CONTOUR LEVELS
0.00000
1.00000
2.00000
3.00000

4.00000
6.00000
7.00000
8.00000
9.00000
10.00000

Leading Edge Sweep = 60 deg.
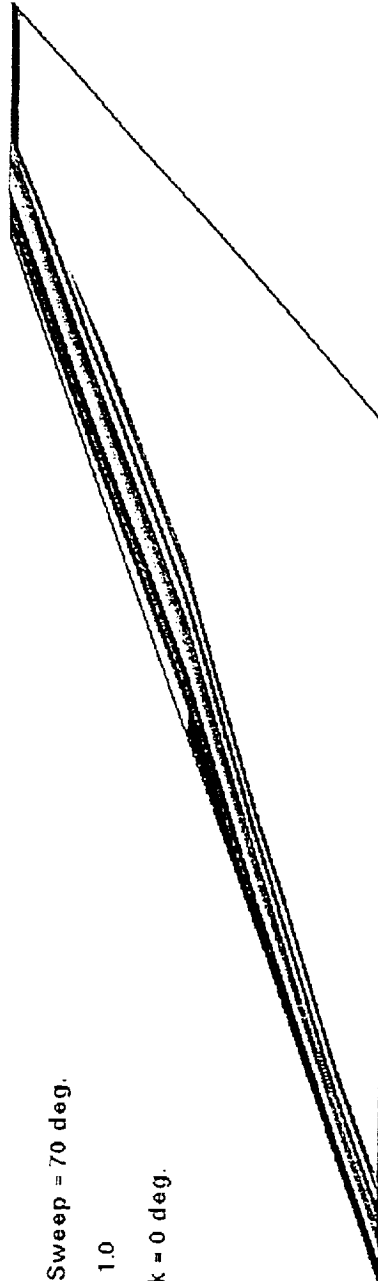
Aspect Ratio = 1.45

Angle Of Attack = 0 deg.

Fig. 6.11   Transition Front Comparison due to Sweep effects on the 1.45 Aspect Ratio Wings
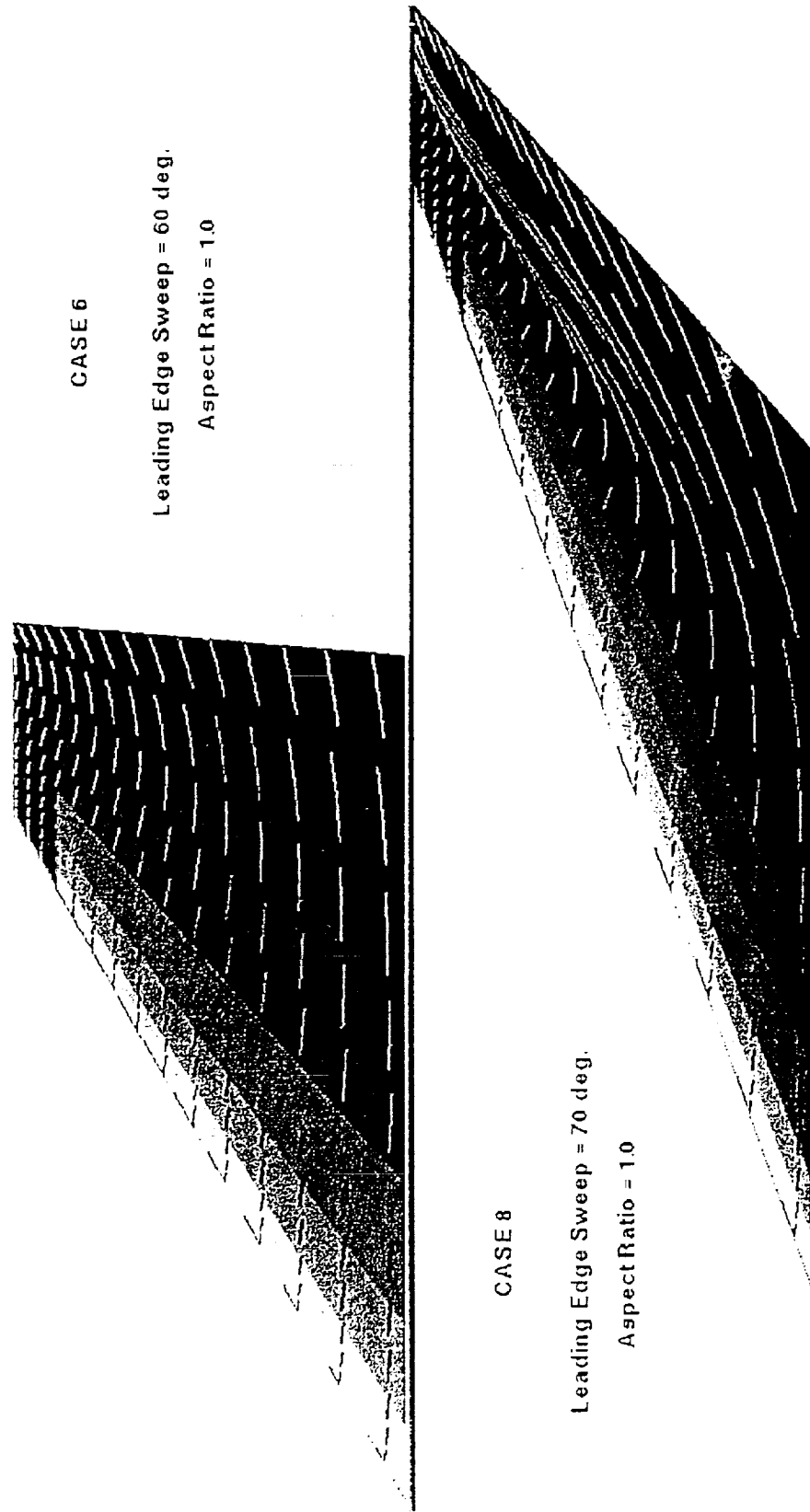
Flow Trace Comparison [Set 1]

CASE 1

Leading Edge Sweep = 45 deg.

Aspect Ratio = 1.0

CASE 4

Leading Edge Sweep = 60 deg.

Aspect Ratio = 1.0
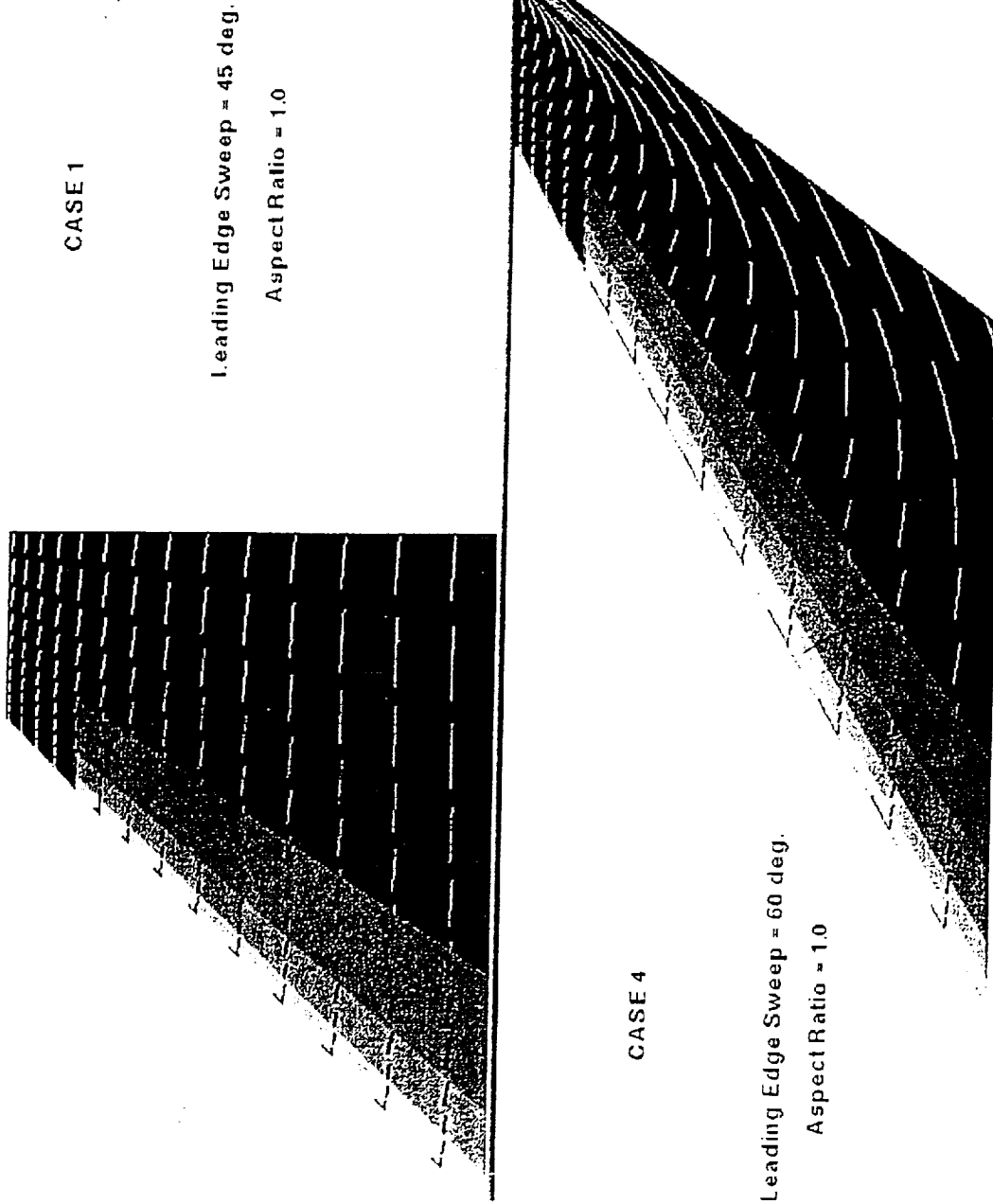
Fig. 6.12 Flow Trace Comparison of the JG45Wing (Case1) and the JG60Wing1 (Case4).

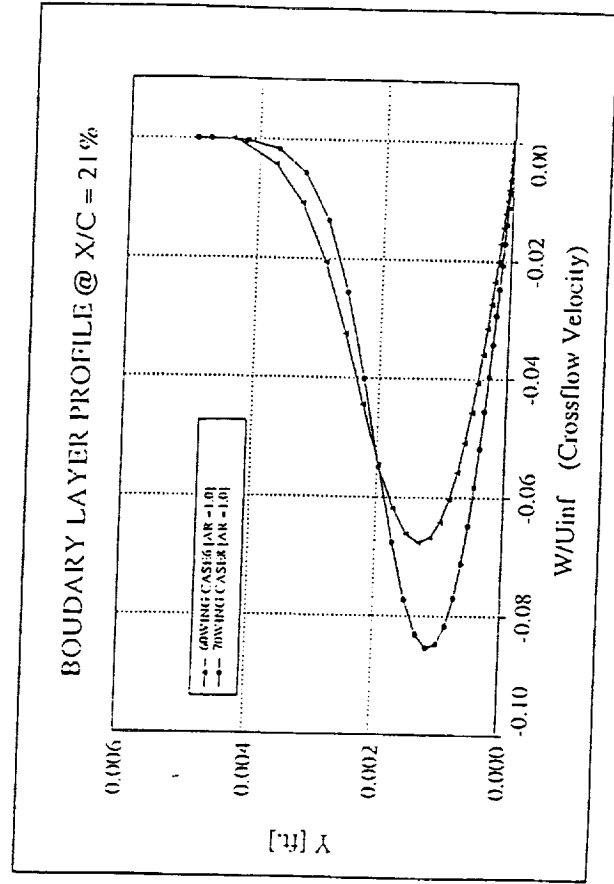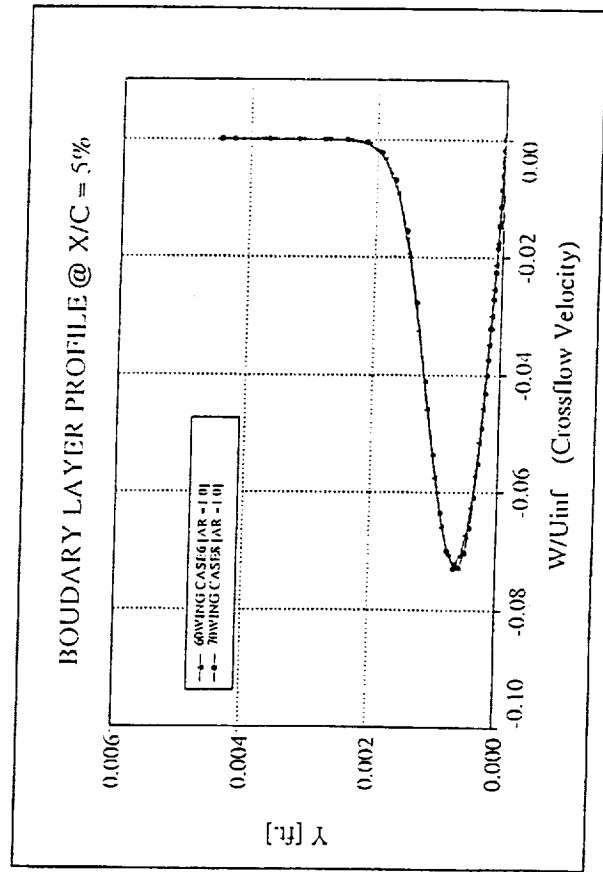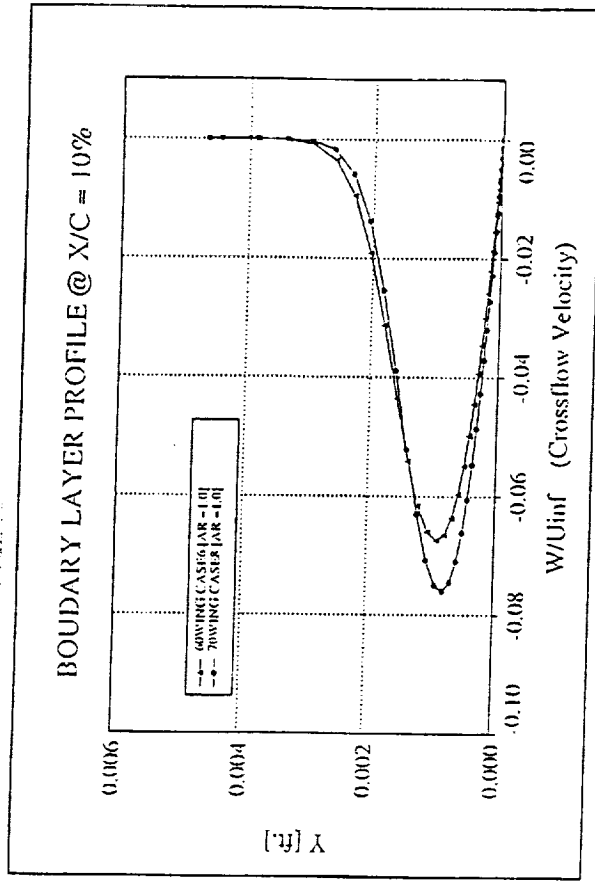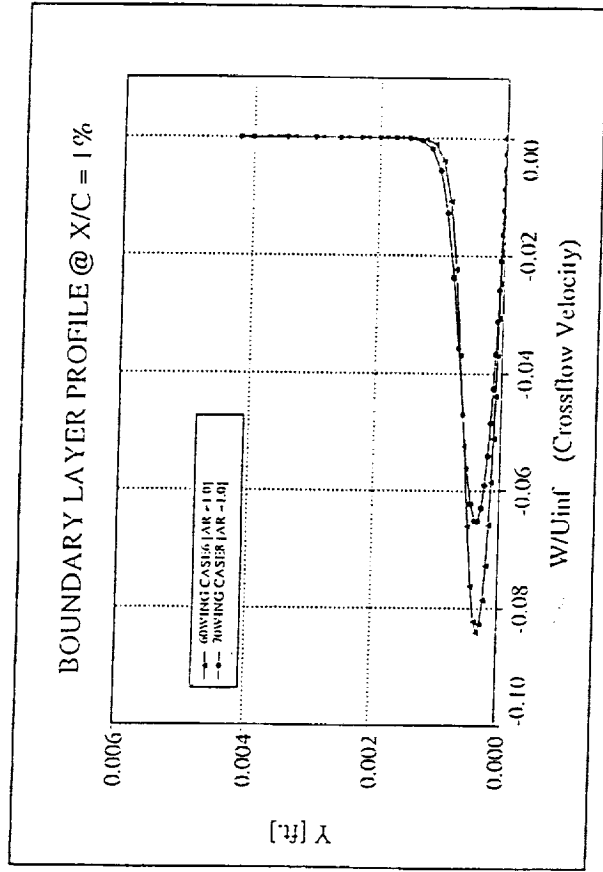# Cross Flow Boundary Layer Profile @ 48% Span
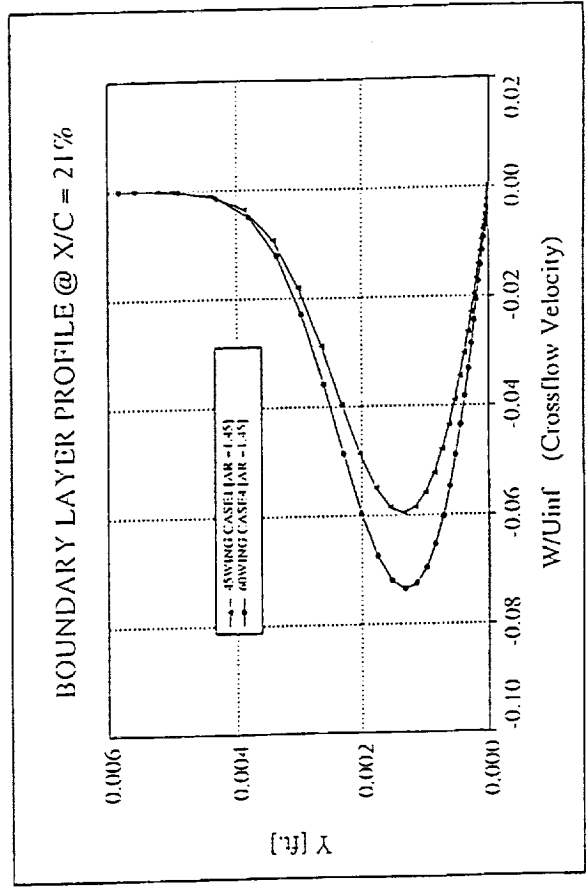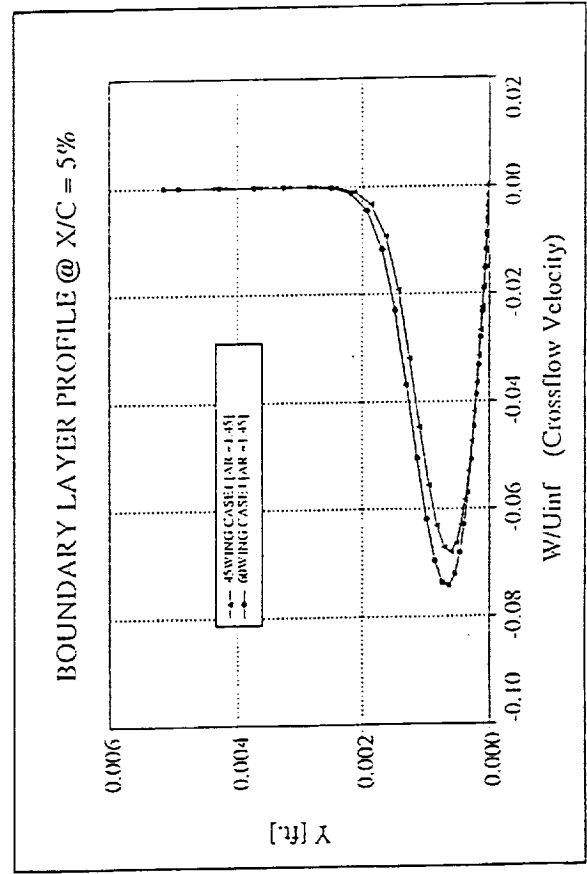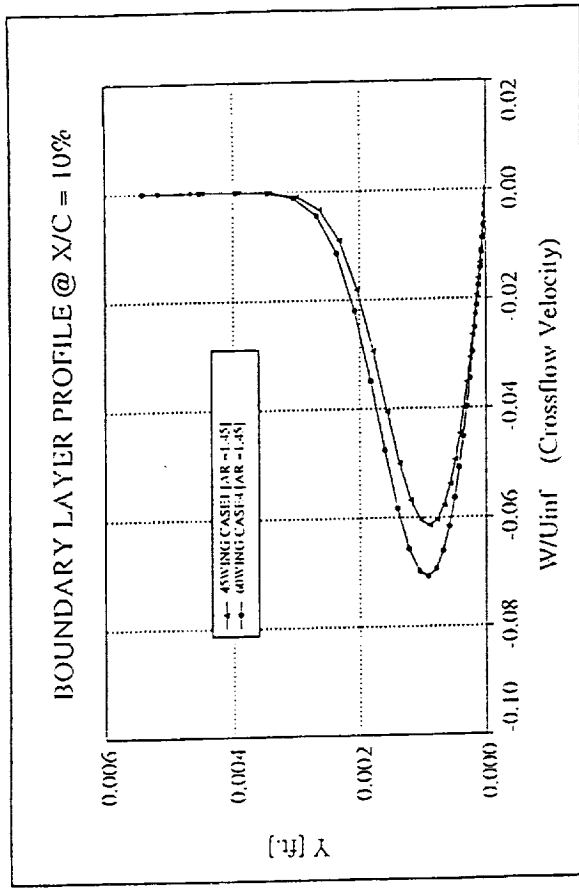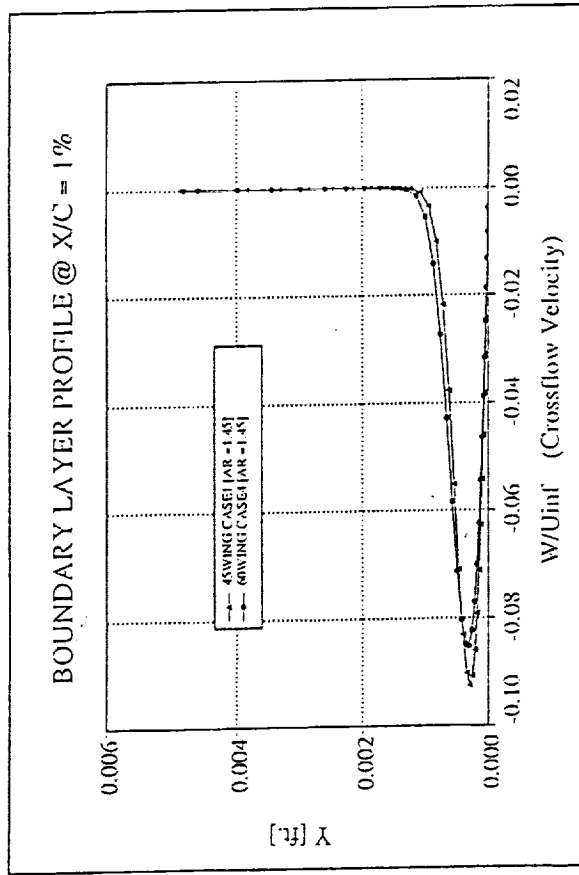
FIG. 6.13 Cross Flow Profile change with sweep @ 48% Span for various airfoil stations.

Maximum Crossflow Effects Due to Sweep at 48% Span

Legend:
45WING CASE1 [AR=1.45]
60WING CASE4 [AR=1.45]

X/C

-W/Uinf max
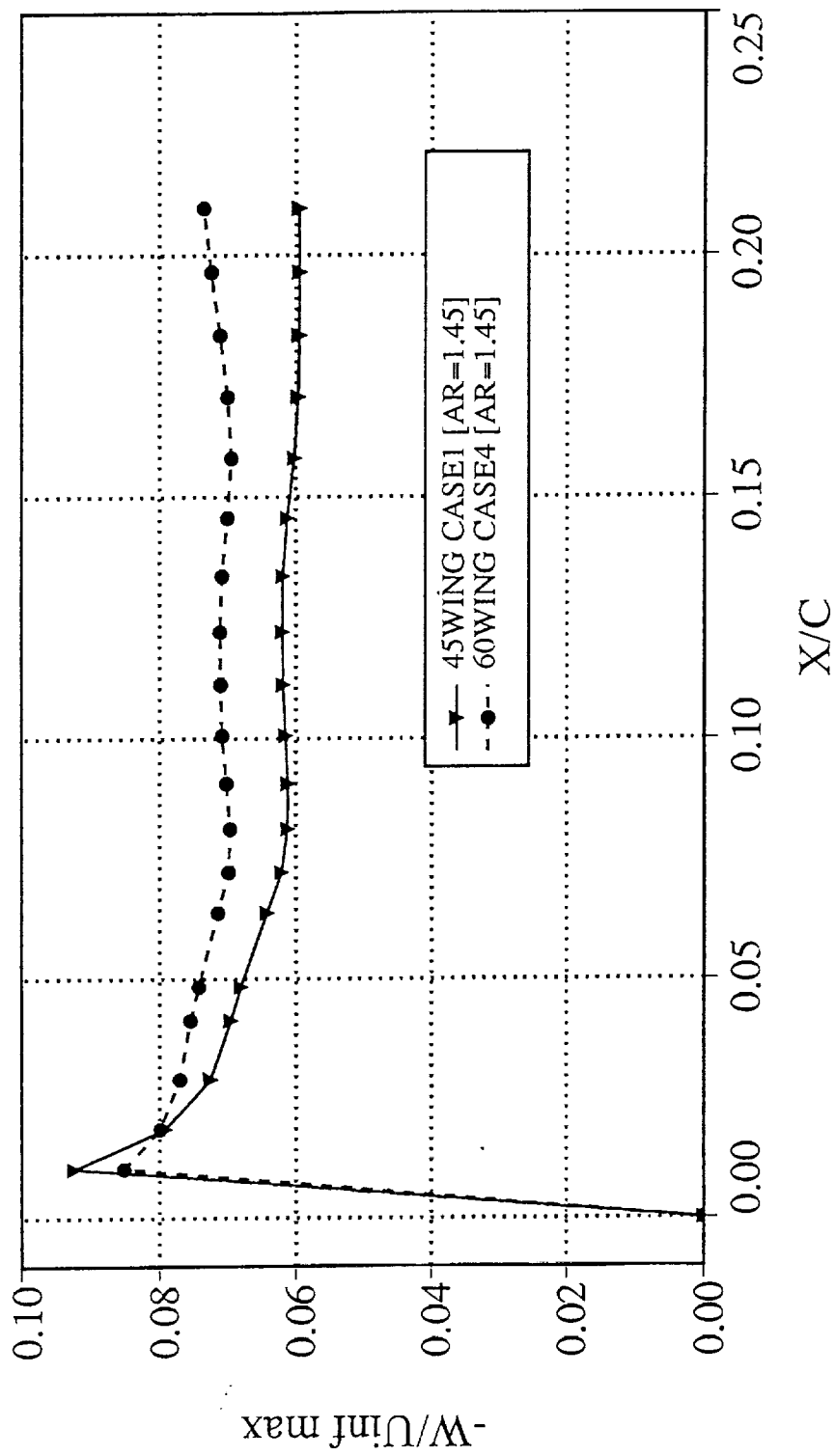
Fig. 6.14

Streamwise Boundary Layer Profile @ 48% Span
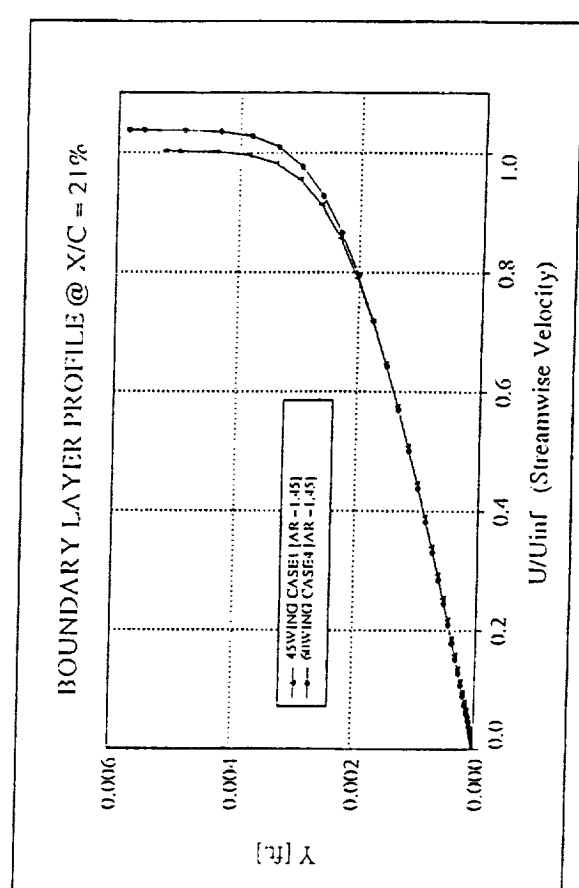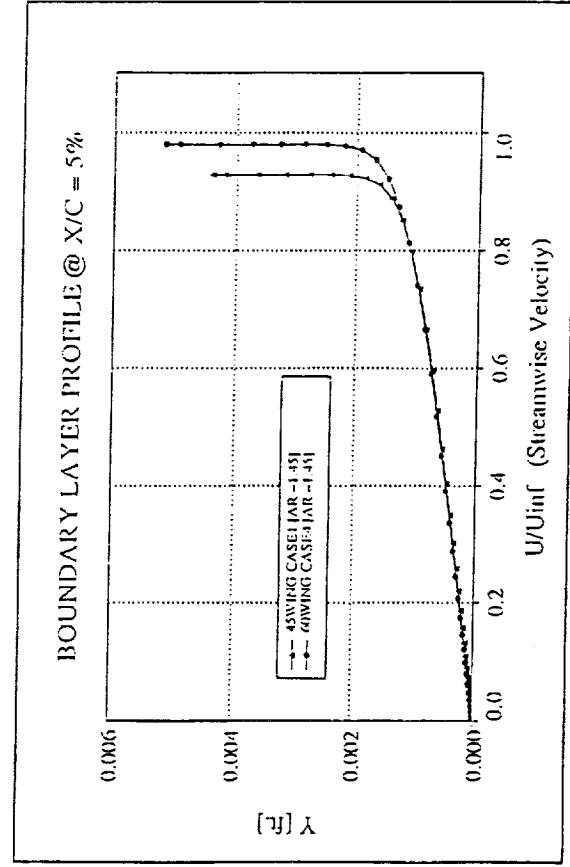
FIG. 6.15 Streamwise Flow Profile change with sweep @ 48% Span for various airfoil stations.

Transition Stablility Curve Comparison
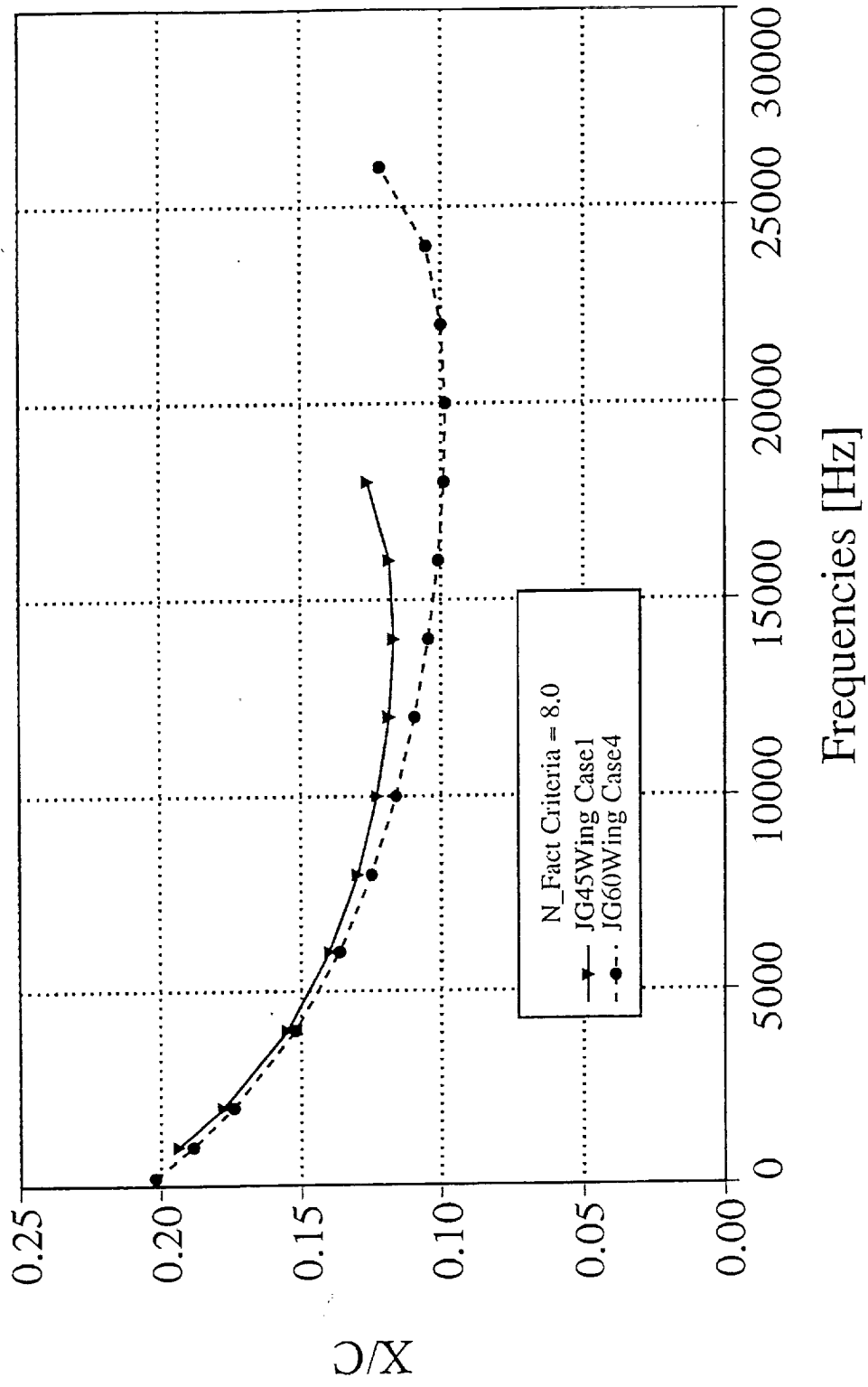
Fig. 6.16

Transition Front Sweep Effects [Set 2]

Leading Edge Sweep = 60 deg.

Aspect Ratio = 1.0

Angle of Attack = 0 deg.

CONTOUR LEVELS
0.00000
1.00000
2.00000
3.00000

4.00000
5.00000
7.00000
8.00000
9.00000
10.00000

Leading Edge Sweep = 70 deg.

Aspect Ratio = 1.0

Angle of Attack = 0 deg.

Fig. 6.17   Transition Front comparison due to sweep effects on the 1.0 Aspect Ratio Wings

Flow Trace Comparison [Set 2]

CASE 6

Leading Edge Sweep = 60 deg.
Aspect Ratio = 1.0

CASE 8

Leading Edge Sweep = 70 deg.
Aspect Ratio = 1.0

Fig. 6.18 Flow Trace comparison of the JG60Wing2 (Case 6) and the JG70Wing (Case 8) configurations

Cross Flow Boundary Layer Profile @ 48% Span

FIG. 6.19 Cross Flow Profile change with sweep @ 48% Span for various airfoil stations.
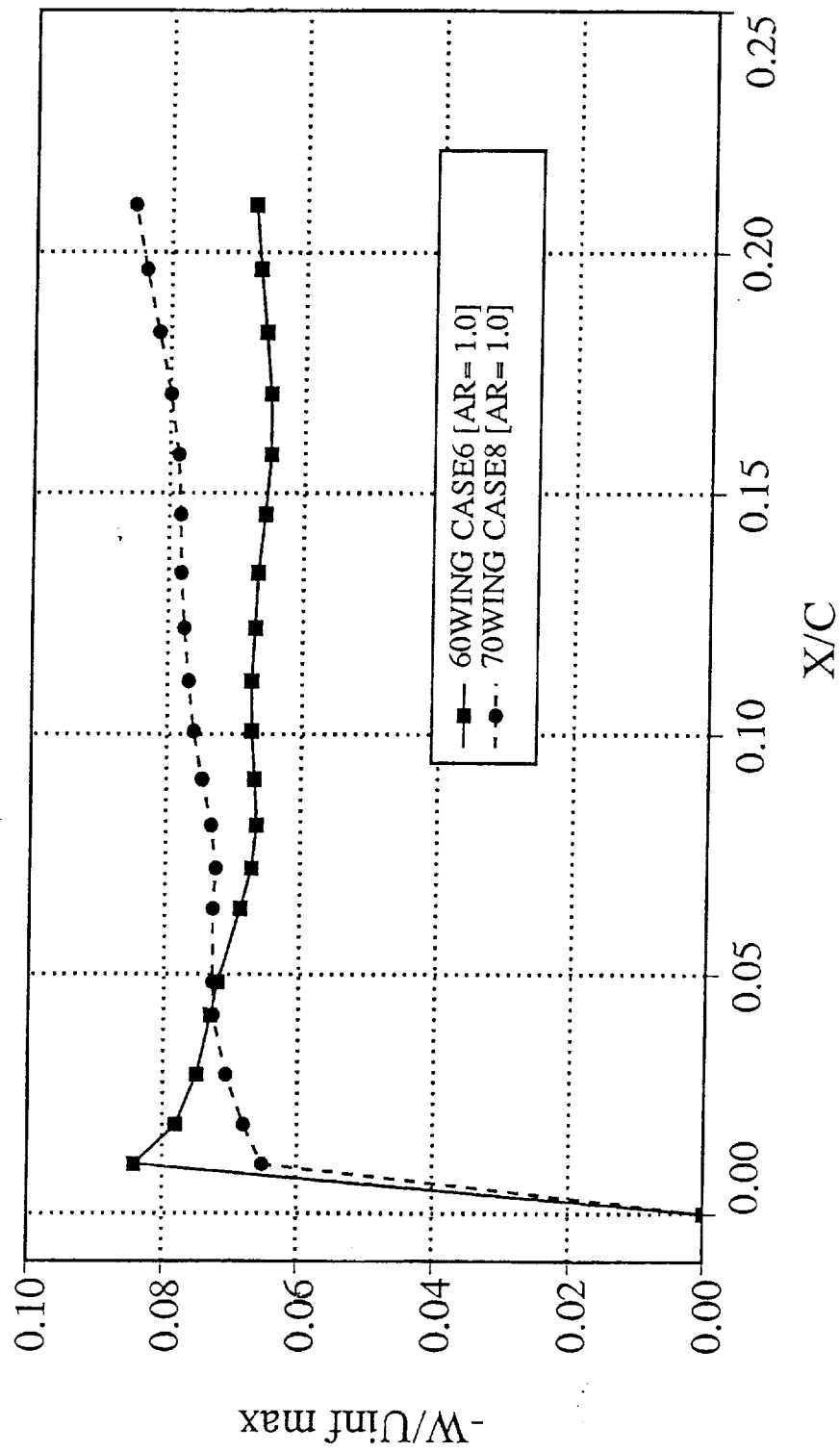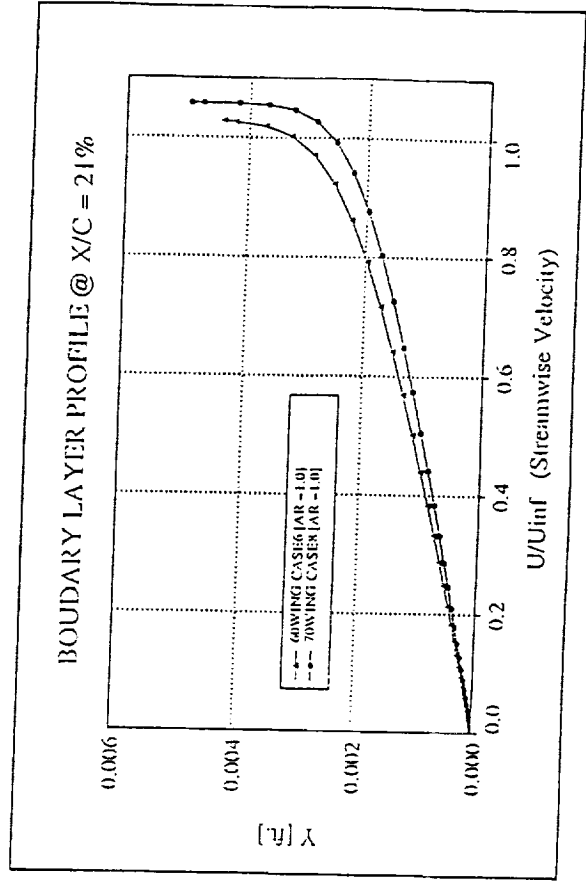
Maximum Crossflow Effects Due to Sweep at 48% Span

Legend:
- 60WING CASE6 [AR= 1.0]
- 70WING CASE8 [AR= 1.0]

X/C

-W/Uinf max

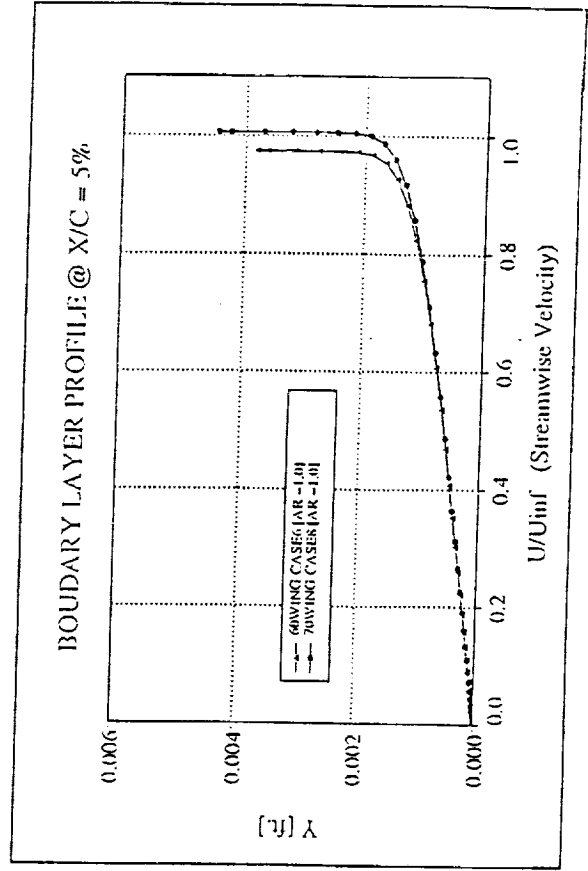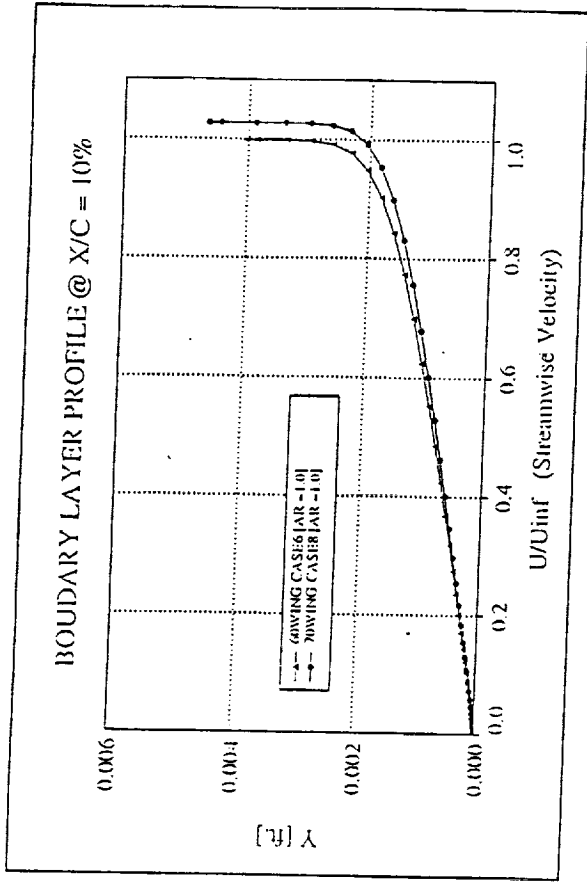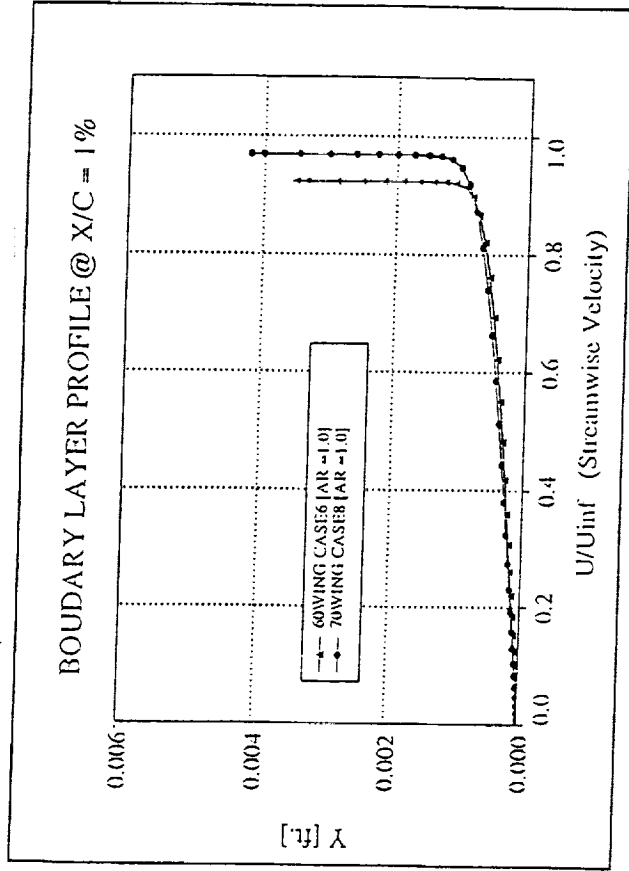Fig. 6.20

Streamwise Boundary Layer Profile @ 48% Span

FIG. 6.21 Streamwise Flow Profile change with sweep @ 48% Span for various airfoil stations.

Transition Stability Curve Results @ 48% Span

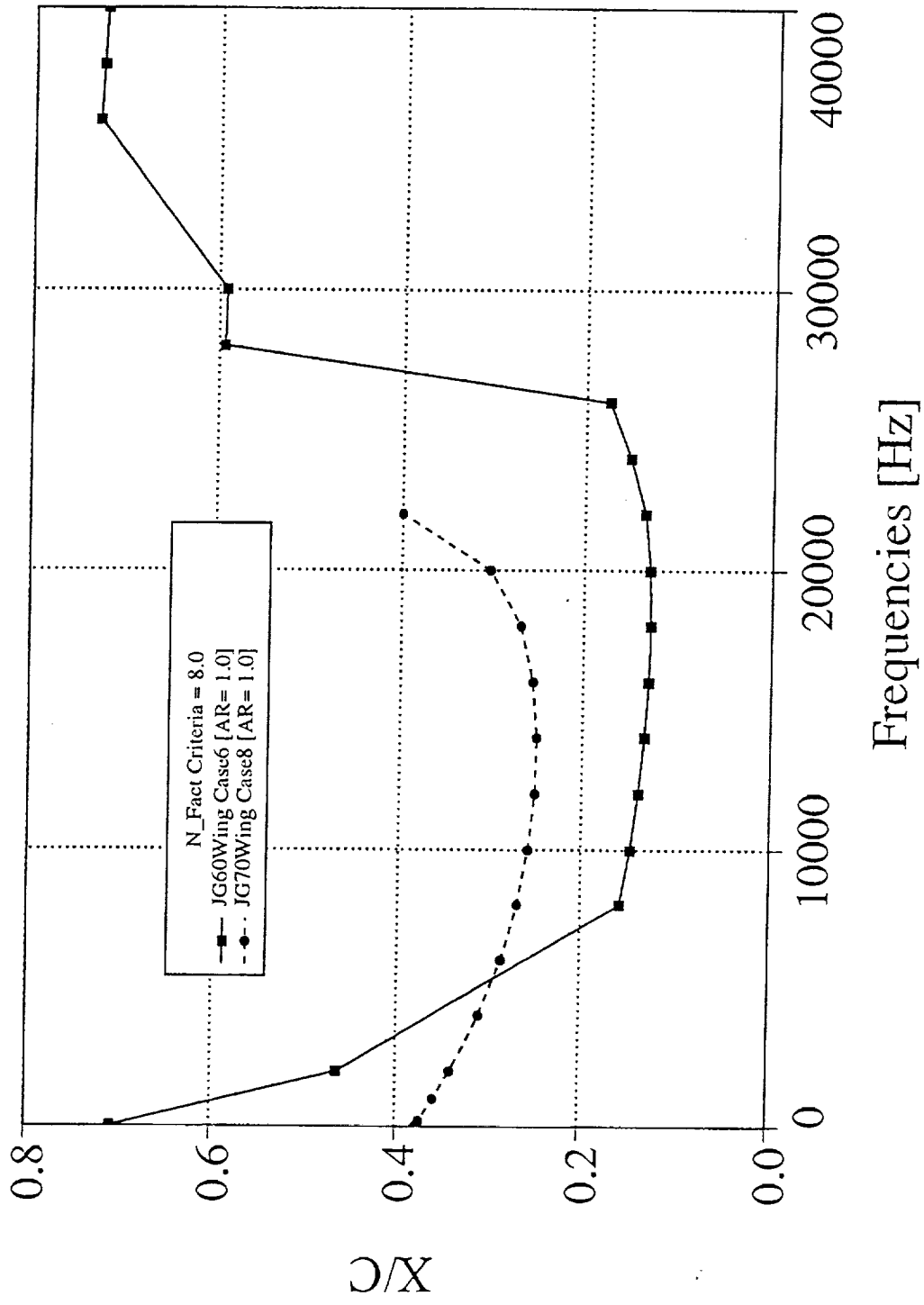N_Fact Criteria = 8.0
——■—— JG60Wing Case6 [AR= 1.0]
--●-- JG70Wing Case8 [AR= 1.0]

X/C

Frequencies [Hz]

Fig. 6.22